EUROPEAN ORGANIZATION FOR NUCLEAR RESEARCH

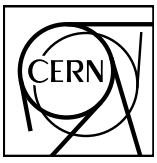

CERN-EP-2016-003
05 January 2016

Multiplicity dependence of charged pion, kaon, and (anti)proton production at large transverse momentum in p–Pb collisions at $\sqrt{s_{\rm NN}}$=5.02 TeV

ALICE Collaboration*

arXiv:1601.03658v2 [nucl-ex] 2 Aug 2016

Abstract

The production of charged pions, kaons and (anti)protons has been measured at mid-rapidity ($-0.5 < y < 0$) in p–Pb collisions at $\sqrt{s_{\rm NN}} = 5.02$ TeV using the ALICE detector at the LHC. Exploiting particle identification capabilities at high transverse momentum ($p_{\rm T}$), the previously published $p_{\rm T}$ spectra have been extended to include measurements up to 20 GeV/c for seven event multiplicity classes. The $p_{\rm T}$ spectra for pp collisions at $\sqrt{s} = 7$ TeV, needed to interpolate a pp reference spectrum, have also been extended up to 20 GeV/c to measure the nuclear modification factor ($R_{\rm pPb}$) in non-single diffractive p–Pb collisions.

At intermediate transverse momentum ($2 < p_{\rm T} < 10$ GeV/c) the proton-to-pion ratio increases with multiplicity in p–Pb collisions, a similar effect is not present in the kaon-to-pion ratio. The $p_{\rm T}$ dependent structure of such increase is qualitatively similar to those observed in pp and heavy-ion collisions. At high $p_{\rm T}$ (> 10 GeV/c), the particle ratios are consistent with those reported for pp and Pb–Pb collisions at the LHC energies.

At intermediate $p_{\rm T}$ the (anti)proton $R_{\rm pPb}$ shows a Cronin-like enhancement, while pions and kaons show little or no nuclear modification. At high $p_{\rm T}$ the charged pion, kaon and (anti)proton $R_{\rm pPb}$ are consistent with unity within statistical and systematic uncertainties.

© 2016 CERN for the benefit of the ALICE Collaboration.
Reproduction of this article or parts of it is allowed as specified in the CC-BY-4.0 license.

*See Appendix A for the list of collaboration members

1 Introduction

In heavy-ion collisions at ultra-relativistic energies, it is well established that a strongly coupled Quark-Gluon-Plasma (sQGP) is formed [1–5]. Some of the characteristic features of the sQGP are strong collective flow and opacity to jets. The collective behavior is observed both as an azimuthal anisotropy of produced particles [6], where the magnitude is described by almost ideal (reversible) hydrodynamics, and as a hardening of p_{T} spectra for heavier hadrons, such as protons, by radial flow [7]. Jet quenching is observed as a reduction of both high p_{T} particles [8, 9] and also fully reconstructed jets [10]. The interpretation of these sQGP properties requires comparisons with reference measurements like pp and p-A collisions. Recent measurements in high multiplicity pp, p-A and d-A collisions at different energies have revealed strong flow-like effects even in these small systems [11–20]. The origin of these phenomena is debated [21–29] and the data reported here provide further inputs to this discussion.

In a previous work, we reported the evidence of radial flow-like patterns in p–Pb collisions [30]. This effect was found to increase with increasing event multiplicity and to be qualitatively consistent with calculations which incorporate the hydrodynamical evolution of the system. It was also discussed that in small systems, mechanisms like color-reconnection may produce radial flow-like effects. The present paper reports complementary measurements covering the intermediate p_{T} region (2–10 GeV/c) and the high-p_{T} region (10–20 GeV/c) exploiting the capabilities of the High Momentum Particle Identification Detector (HMPID) and the Time Projection Chamber (TPC). In this way, high precision measurements are achieved in the intermediate p_{T} region where cold nuclear matter effects like the Cronin enhancement [31, 32] have been reported by previous experiments [33, 34], and where the particle ratios, e.g., the proton (kaon) production relative to that of pions, are affected by large final state effects in central Pb–Pb collisions [35]. Particle ratios are expected to be modified by flow, but hydrodynamics is typically expected to be applicable only up to a few GeV/c [36]. At higher p_{T}, ideas such as parton recombination have been proposed leading to baryon-meson effects [37]. In this way the new dataset complements the lower p_{T} results.

In addition, particle identification at large transverse momenta in p–Pb collisions provides new constraints on the nuclear parton distribution functions (nPDF) which are key inputs in interpreting a large amount of experimental data like d-Au and deep inelastic scattering [38]. Finally, the measurement is also important to study the particle species dependency of the nuclear modification factor (R_{pPb}), to better understand parton energy loss mechanisms in heavy-ion collisions.

In this paper, the charged pion, kaon and (anti)proton R_{pPb} are reported for non-single diffractive (NSD) p–Pb collisions. The pp reference spectra for this measurement were obtained using interpolations of data at different collision energies. The already published p_{T} spectra for inelastic (INEL) pp collisions at $\sqrt{s} = 7$ TeV [39] were extended up to 20 GeV/c and the results are presented here for the first time. These measurements together with the results for INEL pp collisions at $\sqrt{s} = 2.76$ TeV ($p_{\mathrm{T}} < 20$ GeV/c) [35] were used to determine pp reference spectra at $\sqrt{s} = 5.02$ TeV using the interpolation method described in [40].

The paper is organized as follows. In Sec. 2 the ALICE detector as well as the event and track selections are discussed. The analysis procedures for particle identification using the HMPID and TPC detectors are outlined in Sec. 3 and Sec. 4, respectively. Section 5 presents the results and discussions. Finally, Sec. 6 summarizes the main results.

2 Data sample, event and track selection

The results are obtained using data collected with the ALICE detector during the 2013 p–Pb run at $\sqrt{s_{\mathrm{NN}}} = 5.02$ TeV. The detailed description of the ALICE detector can be found in [41] and the performance during run 1 (2009–2013) is described in [42]. Because of the LHC 2-in-1 magnet design,

it is impossible to adjust the energy of the proton and lead-ion beams independently. They are 4 TeV per Z which gives different energies due to the different Z/A of the colliding protons and lead ions. The nucleon-nucleon center-of-mass system is moving in the laboratory frame with a rapidity of $y_{\rm NN}$ = -0.465 in the direction of the proton beam rapidity. In the following, $y_{\rm lab}$ ($\eta_{\rm lab}$) are used to indicate the (pseudo)rapidity in the laboratory reference frame, whereas y (η) denotes the (pseudo)rapidity in the center-of-mass reference system where the Pb beam is assigned positive rapidity.

In the analysis of the p–Pb data, the event selection follows that used in the analysis of inclusive charged particle production [43]. The minimum bias (MB) trigger signal was provided by the V0 counters [44], which contain two arrays of 32 scintillator tiles each covering the full azimuth within $2.8 < \eta_{\rm lab} < 5.1$ (V0A) and $-3.7 < \eta_{\rm lab} < -1.7$ (V0C). The signal amplitude and arrival time collected in each tile were recorded. A coincidence of signals in both V0A and V0C detectors was required to remove contamination from single diffractive and electromagnetic events. In the offline analysis, background events were further suppressed by requiring the arrival time of signals on the neutron Zero Degree Calorimeter A, which is positioned in the Pb-going direction, to be compatible with a nominal p–Pb collision occurring close to the nominal interaction point. The estimated mean number of interactions per bunch crossing was below 1% in the sample chosen for this analysis. Due to the weak correlation between collision geometry and multiplicity, the particle production in p–Pb collisions is studied in event multiplicity classes instead of centralities [45]. The multiplicity classes are defined using the total charge deposited in the V0A detector as in [30], where V0A is positioned in the Pb-going direction. The MB results have been normalized to the total number of NSD events using a trigger and vertex reconstruction efficiency correction which amounts to $3.6\,\% \pm 3.1\,\%$ [46]. The multiplicity dependent results have been normalized to the visible (triggered) cross-section correcting for the vertex reconstruction efficiency (this was not done in [30]). This correction is of the order of 5% for the lowest V0A multiplicity class (80–100%) and negligible for the other multiplicity classes ($< 1\%$).

In the $\sqrt{s} = 7$ TeV pp analysis the MB trigger required a hit in the two innermost layers of the Inner Tracking System (ITS), the Silicon Pixel Detector (SPD), or in at least one of the V0 scintillator arrays in coincidence with the arrival of proton bunches from both directions. The offline analysis to eliminate background was done using the time information provided by the V0 detectors in correlation with the number of clusters and tracklets[1] in the SPD.

Tracks are required to be reconstructed in both the ITS and the TPC. Additional track selection criteria are the same as in [47] and based on the number of space points, the quality of the track fit, and the distance of closest approach to the reconstructed collision vertex. Charged tracks where the identity of the particle has changed due to a weak decay, e.g., $\mathrm{K}^- \to \mu^- + \bar{\nu}_\mu$, are identified by the tracking algorithm due to their distinct kink topologies [48] and rejected in this analysis. The remaining contamination is negligible ($\ll$1%). In order to have the same kinematic coverage as used in the p–Pb low $p_{\rm T}$ analysis [30], the tracks were selected in the pseudorapidity interval $-0.5 < \eta < 0$. In addition, for the HMPID analysis it is required that the tracks are propagated and matched to a primary ionization cluster in the Multi-Wire Proportional Chamber (MWPC) gap of the HMPID detector [39, 47].

The published results of charged pion, kaon and (anti)proton production at low $p_{\rm T}$ for pp [39] and p–Pb [30] collisions at $\sqrt{s} = 7$ TeV and $\sqrt{s_{\rm NN}} = 5.02$ TeV, respectively, used different Particle IDentification (PID) detectors and techniques. A summary of the $p_{\rm T}$ ranges covered by the published analyses and the analyses presented in this paper can be found in Table 1.

In the following, the analysis techniques used to obtain the identified particle $p_{\rm T}$ spectra in the intermediate and high-$p_{\rm T}$ ranges using HMPID and TPC will be discussed.

[1] Tracklets are pairs of hits from the two layers of the SPD which make a line pointing back to the collision vertex.

	Analysis	$\pi^+ + \pi^-$	$\mathrm{K}^+ + \mathrm{K}^-$	$\mathrm{p} + \bar{\mathrm{p}}$
pp	Published [39]*	0.1 – 3.0	0.2 – 6.0	0.3 – 6.0
	TPC dE/dx rel. rise	2 – 20	3 – 20	3 – 20
p–Pb	Published [30]†	0.1 – 3.0	0.2 – 2.5	0.3 – 4.0
	HMPID	1.5 – 4.0	1.5 – 4.0	1.5 – 6.0
	TPC dE/dx rel. rise	2 – 20	3 – 20	3 – 20

* Included detectors: ITS, TPC, Time-of-Flight (TOF), HMPID. The results also include the kink-topology identification of the weak decays of charged kaons.

† Included detectors: ITS, TPC, TOF.

Table 1: Transverse momentum ranges (GeV/c) covered by the individual and combined analyses for pp collisions at $\sqrt{s} = 7$ TeV and p–Pb collisions at $\sqrt{s_{\mathrm{NN}}} = 5.02$ TeV.

3 HMPID analysis

The HMPID detector [49] is located about 5 m from the beam axis, covering a limited acceptance of $|\eta_{\mathrm{lab}}| < 0.5$ and $1.2^\circ < \phi < 58.5^\circ$, that corresponds to ∼5% of the TPC geometrical acceptance (2π in azimuthal angle and the pseudo-rapidity interval $|\eta| < 0.9$ [50]) for high p_{T} tracks. The HMPID analysis uses $\sim 9\times10^7$ minimum-bias p–Pb events at $\sqrt{s_{\mathrm{NN}}} = 5.02$ TeV. The event and track selection and the analysis technique are similar to those described in [39, 47]. It is required that tracks are propagated and matched to a primary ionization cluster in the Multi-Wire Proportional Chamber (MWPC) gap of the HMPID detector. The PID in the HMPID is done by measuring the Cherenkov angle, θ_{Ch} [49]:

$$\cos\theta_{\mathrm{Ch}} = \frac{1}{n\beta} \Longrightarrow \theta_{\mathrm{Ch}} = \arccos\left(\frac{\sqrt{p^2+m^2}}{np}\right), \tag{1}$$

where n is the refractive index of the radiator used (liquid C_6F_{14} with n = 1.29 at E_{ph} = 6.68 eV and temperature $T = 20$ °C), p and m are the momentum and the mass of the given particle, respectively. The measurement of the single photon θ_{Ch} angle in the HMPID requires the knowledge of the track parameters, which are estimated by the track extrapolation from the central tracking detectors up to the radiator volume, where the Cherenkov photons are emitted. Only one charged particle cluster is associated to each extrapolated track, selected as the closest cluster to the extrapolated track point on the cathode plane. To reject the fake cluster-match associations in the detector, a selection on the distance $d_{(\mathrm{track-MIP})}$ computed on the cathode plane between the track extrapolation point and the reconstructed charged-particle cluster position is applied. The distance has to be less than 5 cm, independent of track momentum. Starting from the photon cluster coordinates on the photocathode, a back-tracking algorithm calculates the corresponding emission angle. The Cherenkov photons are selected by the Hough Transform Method (HTM) [51] that discriminates the signal from the background. For a given track, the Cherenkov angle θ_{Ch} is then computed as the weighted mean of the single photon angles selected by the HTM. Figure 1 shows the θ_{Ch} as a function of the track momentum. The reconstructed angle distribution for a given momentum interval is fitted by a sum of three Gaussian distributions, corresponding to the signals from pions, kaons, and protons. The fitting is done in two steps. In the first step the initial values of fit parameters are set to the expected values. The mean values, $\langle\theta_{\mathrm{Ch}}\rangle_i$, are obtained from Eq. 1, tuning the refractive index to match the observed Cherenkov angles, and the resolution values are taken from a Monte Carlo simulation of the detector response. After this first step, the p_{T} dependences of the mean and width are fitted with the function given by Eq. 1 and a polynomial one, respectively. In the second step, the fitting is repeated with the yields as the only free parameters, constraining the mean and resolution values to the fitted value. The second iteration is particularly important at high p_{T} where the separation between different species is reduced. Figure 2 gives examples of fits to the reconstructed

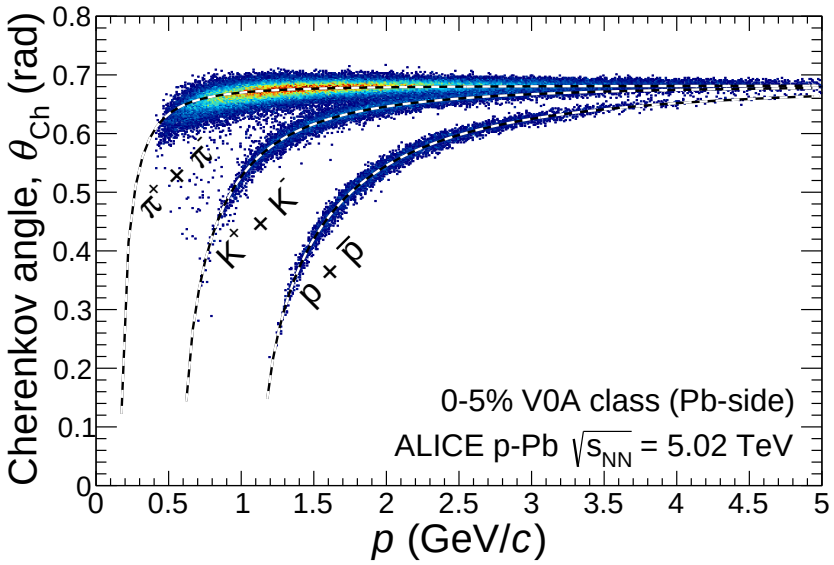

Fig. 1: (Color online.) Cherenkov angle measured in the HMPID as a function of the track momentum in p–Pb collisions at $\sqrt{s_{\rm NN}} = 5.02$ TeV for the 0–5% V0A multiplicity class (see the text for further details). The dashed lines represent the expected curves calculated using Eq. 1 for each particle species.

Cherenkov angle distributions in two narrow $p_{\rm T}$ intervals for the 0–5% multiplicity class. The raw yields are then corrected by the total reconstruction efficiency given by the convolution of the tracking, PID efficiency, and distance cut correction. The tracking efficiency, convoluted with the geometrical acceptance of the detector, has been evaluated using Monte Carlo simulations. For all three particle species this efficiency increases from ∼5% at 1.5 GeV/c up to ∼6% at high $p_{\rm T}$. The PID efficiency is determined by the Cherenkov angle reconstruction efficiency. It has been computed by means of Monte-Carlo simulations and it reaches ∼90% for particles with velocity $\beta\sim1$, with no significant difference between positive and negative tracks. The distance cut correction, defined as the ratio between the number of the tracks that pass the cut on $d_{\rm (track-MIP)}$ and all the tracks in the detector acceptance, has been evaluated from data. It is momentum dependent, and it is equal to ∼53% at 1.5 GeV/c, reaches ∼70% for particles with velocity $\beta\sim1$. A small difference between positive and negative tracks is present; negative tracks having a distance correction ∼2% lower than the positive ones. This effect is caused by a radial residual misalignment of the HMPID chambers and an imperfect estimation of the energy loss in the material traversed by the track. Tracking efficiency, PID efficiency and distance cut correction do not show variation with the event track multiplicity.

3.1 Systematic uncertainties

The systematic uncertainty on the results of the HMPID analysis has contributions from tracking, PID and tracks association [39, 47]. The uncertainties related to the tracking have been estimated by changing the track selection cuts individually, e.g. the number of crossed readout rows in the TPC and the value of the track's χ^2 normalized to the number of TPC clusters. To estimate the PID contribution, the parameters (mean and resolution) of the fit function used to extract the raw yields were varied by a reasonable quantity, leaving them free in a given range; the range chosen for the mean values is $[\langle\theta_{\rm Ch}\rangle - \sigma, \langle\theta_{\rm Ch}\rangle + \sigma]$ and for the resolution $[\sigma - 0.1\sigma, \sigma + 0.1\sigma]$. A variation of 10% of the resolution corresponds to its maximum expected variation when taking into account the different running conditions of the detector during data taking which have an impact on its performance. When the means are changed, the resolution values are fixed to the default value and vice versa. The variation of parameters is done for the three Gaussians (corresponding to the three particle species) simultaneously. In addition, the uncertainty of

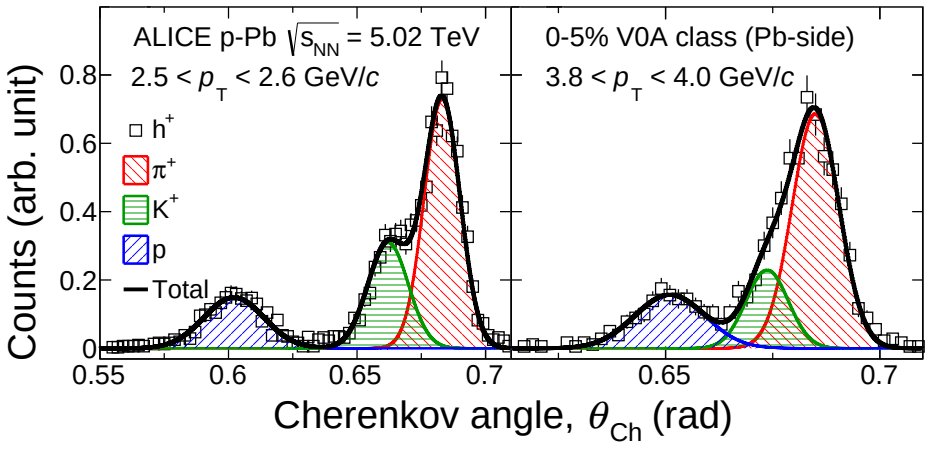

Fig. 2: (Color online.) Distributions of the Cherenkov angle measured in the HMPID for positive tracks having p_{T} between 2.5–2.6 GeV/c (left) and between 3.8–4.0 GeV/c (right), in p–Pb collisions at $\sqrt{s_{\mathrm{NN}}} = 5.02$ TeV for the 0–5% V0A multiplicity class (see the text for further details).

Effect	$\pi^+ + \pi^-$		$\mathrm{K}^+ + \mathrm{K}^-$		$\mathrm{p} + \bar{\mathrm{p}}$	
p_{T} value (GeV/c)	2.5	4	2.5	4	2.5	4
PID	6%	12%	6%	12%	4%	5%
Tracking efficiency	6%		6%		7%	
Distance cut correction	6%	2%	6%	2%	4%	2%

Table 2: Main sources of systematic uncertainties for the HMPID p–Pb analysis.

the association of the track to the charged particle signal is obtained by varying the default value of the distance cut required for the match by $\pm$ 1 cm. These contributions do not vary with the collision multiplicity. A summary of the different contributions to the systematic uncertainty for the HMPID p–Pb analysis is shown in Table 2.

4 TPC dE/dx relativistic rise analysis

The relativistic rise regime of the specific energy loss, dE/dx, measured by the TPC allows identification of charged pions, kaons, and (anti)protons up to $p_{\mathrm{T}} = 20$ GeV/c. The results presented in this paper were obtained using the method detailed in [47]. In this analysis, around 8×10^7 (4.7×10^7) p–Pb (pp) MB triggered events were used. The event and track selection has already been discussed in Section 2.

As discussed in [47], the dE/dx is calibrated taking into account chamber gain variations, track curvature and diffusion, to obtain a response that essentially only depends on $\beta\gamma$. Inherently, tracks at forward rapidity will have better resolution due to longer integrated track-lengths, so in order to analyze homogeneous samples the analysis is performed in four η intervals. Samples of topologically identified pions (from $\mathrm{K}^0_{\mathrm{S}}$ decays), protons (from Λ decays) and electrons (from γ conversions) were used to parametrize the Bethe-Bloch response, $\langle \mathrm{d}E/\mathrm{d}x \rangle$ ($\beta\gamma$), and the relative resolution, $\sigma_{\mathrm{d}E/\mathrm{d}x}$ ($\langle \mathrm{d}E/\mathrm{d}x \rangle$) [47]. For the p–Pb data, these response functions are found to be slightly multiplicity dependent (the $\langle \mathrm{d}E/\mathrm{d}x \rangle$ changes by $\sim$0.4% and the sigma by $\sim$2.0%). However, a single set of functions is used for all multiplicity intervals, and the dependence is included in the systematic uncertainties. Figure 3 shows dE/dx as a function of momentum for p–Pb events. The characteristic separation power between particle species in number of standard deviations (S_σ) as a function of p, is shown in Fig. 4 for minimum bias p–Pb collisions. For example, S_σ for pions and kaons is calculated as:

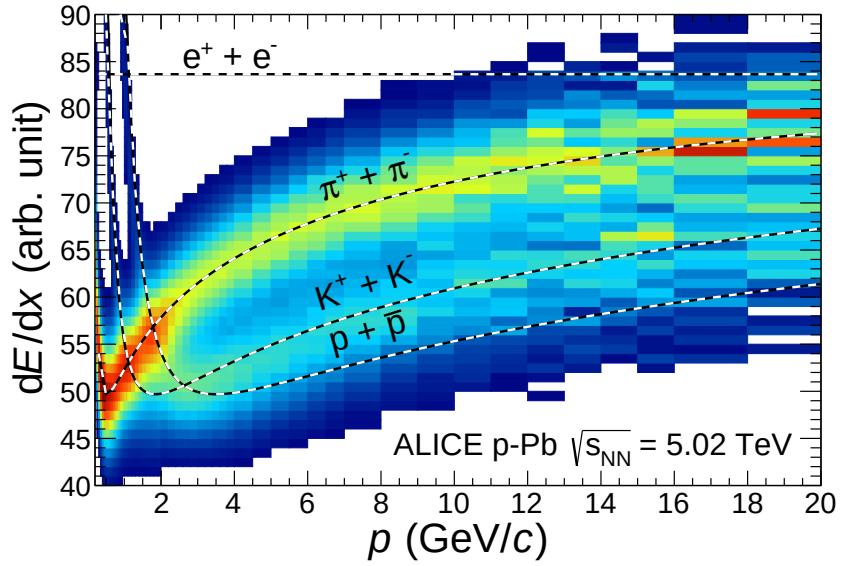

Fig. 3: (Color online.) Specific energy loss, $\mathrm{d}E/\mathrm{d}x$, as a function of momentum p in the pseudorapidity range $-0.5 < \eta < -0.375$ for minimum bias p–Pb collisions. In each momentum bin the $\mathrm{d}E/\mathrm{d}x$ spectra have been normalized to have unit integrals and only bins with more than 2% of the counts are shown (making electrons not visible in the figure, except at very low momentum). The curves show the $\langle \mathrm{d}E/\mathrm{d}x \rangle$ response for pions, kaons, protons and electrons.

$$S_\sigma = \frac{\left\langle \frac{\mathrm{d}E}{\mathrm{d}x} \right\rangle_{\pi^+ + \pi^-} - \left\langle \frac{\mathrm{d}E}{\mathrm{d}x} \right\rangle_{\mathrm{K}^+ + \mathrm{K}^-}}{0.5\,(\sigma_{\pi^+ + \pi^-} + \sigma_{\mathrm{K}^+ + \mathrm{K}^-})}. \tag{2}$$

The separation in number of standard deviations is the largest (smallest) between pions and protons (kaons and protons) and it is nearly constant at large momenta.

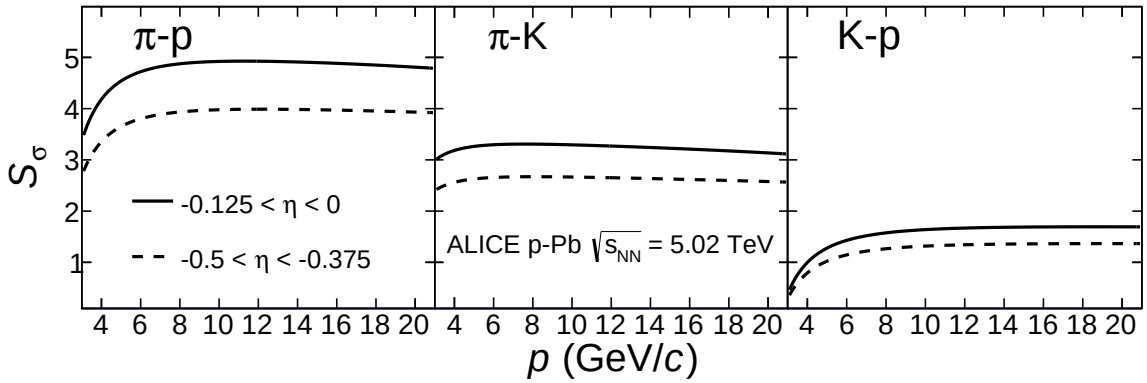

Fig. 4: Separation in number of standard deviations between: pions and protons (left panel), pions and kaons (middle panel), and kaons and protons (right panel). Results for minimum bias p–Pb data and for two specific pseudorapidity intervals are shown. More details can be found in [47].

The main part of this analysis is the determination of the relative particle abundances, hereafter called particle fractions, which are defined as the $\pi^+ + \pi^-$, $\mathrm{K}^+ + \mathrm{K}^-$, $\mathrm{p} + \bar{\mathrm{p}}$ and $e^+ + e^-$ yields normalized to that for inclusive charged particles. Since the TPC $\mathrm{d}E/\mathrm{d}x$ signal is Gaussian distributed as illustrated in [47], particle fractions are obtained using four-Gaussian fits to $\mathrm{d}E/\mathrm{d}x$ distributions in η and p intervals. The parameters (mean and width) of the fits are fixed using the parametrized Bethe-Bloch and resolution

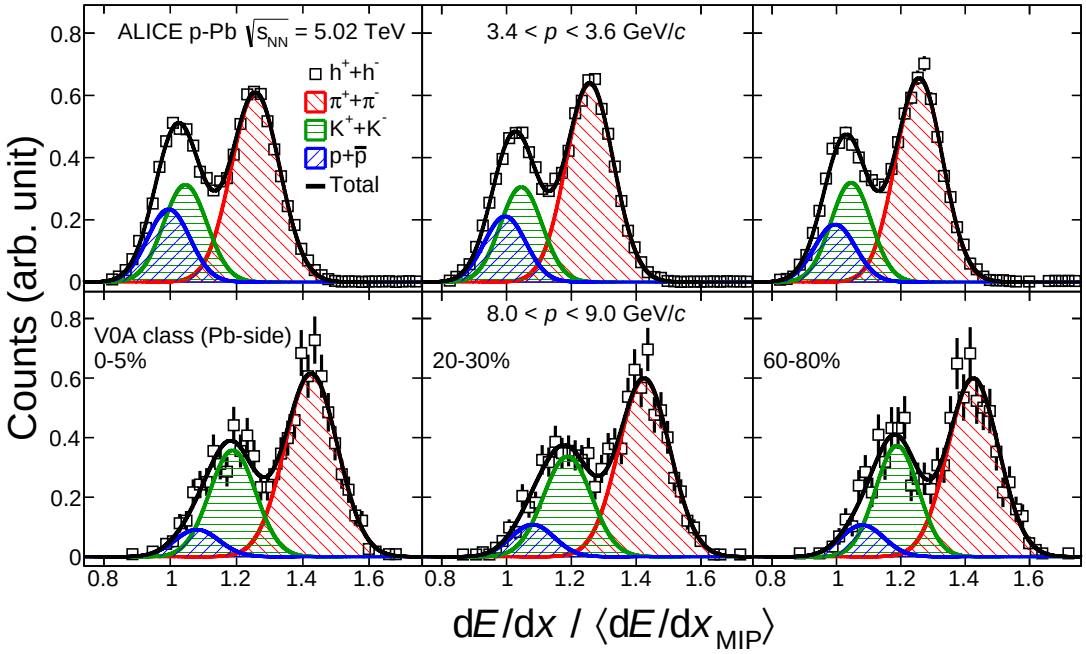

Fig. 5: (Color online.) Four-Gaussian fits (lines) to the dE/dx spectra (markers) for tracks having momentum $3.4 < p < 3.6$ GeV/c (top row) and $8.0 < p < 9.0$ GeV/c (bottom row) within $-0.125 < \eta < 0$. All of the spectra are normalized to have unit integrals. Columns refer to different V0A multiplicity classes. Individual signals of charged pions, kaons, and (anti)protons are shown as red, green, and blue dashed areas, respectively. The contribution of electrons is not visible and is negligible ($< 1\%$).

curves mentioned earlier. Examples of these fits can be seen in Fig. 5 for two momentum intervals, $3.4 < p < 3.6$ GeV/c and $8 < p < 9$ GeV/c. The particle fractions in a p_{T} range, are obtained as the weighted average of the contributing p intervals. Since the particle fractions as a function of p_{T} are found to be independent of η, they are averaged. The particle fractions measured in p–Pb and pp collisions are corrected for relative efficiency differences using DPMJET [52] and PHOJET [53] Monte Carlo (MC) generators, respectively. Furthermore, the relative pion and proton abundances were corrected for the contamination of secondary particles (feed-down), more details of the method can be found in [47].

The invariant yields, $1/(2\pi p_{\mathrm{T}})\,\mathrm{d}^2N/\mathrm{d}y\mathrm{d}p_{\mathrm{T}}$, are constructed using two components: the corrected particle fractions and the corrected invariant charged particle yields. For the pp analysis at $\sqrt{s} = 7$ TeV, the latter component was taken directly from the published results for inclusive charged particles [40]. However, analogous results for p–Pb data are neither available for neither the kinematic range $-0.5 < y < 0$ nor for the different multiplicity classes [54], they were therefore measured here and the results used to determine the invariant yields.

4.1 Systematic uncertainties

The systematic uncertainties mainly consist of two components: the first is due to the event and track selection, and the second one is due to the PID. The first component was obtained from the analysis of inclusive charged particles [40, 54]. For INEL pp collisions at 7 TeV, the systematic uncertainties have been taken from [40]. For p–Pb collisions, there are no measurements in the η interval reported here ($-0.5 < \eta < 0$); however, it has been shown that the systematic uncertainty exhibits a negligible dependence on η and multiplicity [45]. Therefore, the systematic uncertainties reported in [54] have been assigned to the identified charged hadron p_{T} spectra for all the V0A multiplicity classes.
The second component was measured following the procedure described in [47], where the largest contribution is attributed to the uncertainties in the parameterization of the Bethe-Bloch and resolution curves

		pp collisions									
		$\pi^+ + \pi^-$		$K^+ + K^-$		$p + \bar{p}$		K/π		p/π	
	p_T (GeV/c)	2.0	10	3.0	10	3.0	10	3.0	10	3.0	10
	Uncertainty										
	Event and track selection*	7.3%		7.3%		7.3%		–		–	
	Feed-down correction	0.2%		–		1.2%		0.2%		1.2%	
	Efficiency correction	3.2%		3.2%		3.2%		4.5%		4.5%	
	Correction for muons	0.3%	0.5%	–		–		0.3%	0.5%	0.3%	0.5%
	Parametrization of Bethe-Bloch and resolution curves	1.8%	1.9%	20%	6.9%	24%	15%	17%	9.0%	17%	19%
		p–Pb collisions									
	Uncertainty										
	Event and track selection*	3.3%	3.6%	3.3%	3.6%	3.3%	3.6%	–		–	
	Feed-down correction	$\leq 0.2\%$		–		2.6%	0.7%	$\leq 0.2\%$		2.6%	0.7%
	Efficiency correction	3.2%		3.2%		3.2%		4.5%		4.5%	
	Correction for muons†	0.3%	0.4%	–		–		0.3%	0.4%	0.3%	0.4%
	Parametrization of Bethe-Bloch and resolution curves										
Multiplicity classes	**0-5 %**	1.7%	1.9%	17%	8.0%	15%	13%	16%	10.4%	12%	11%
	5-10 %	1.7%	2.0%	17%	5.6%	16%	12%	18%	7.2%	14%	24%
	10-20 %	1.6%	1.9%	16%	7.2%	16%	12%	18%	9.5%	16%	15%
	20-40 %	1.6%	2.0%	16%	6.7%	17%	15%	18%	8.0%	17%	18%
	40-60 %	1.5%	1.9%	15%	6.5%	17%	12%	18%	8.3%	18%	13%
	60-80 %	1.6%	1.8%	16%	6.3%	20%	13%	21%	8.3%	22%	18%
	80-100 %	1.4%	1.5%	13%	5.9%	20%	13%	16%	7.3%	23%	21%

* Common to all species, values taken from [40, 54].
† Found to be multiplicity independent.

Table 3: Summary of the systematic uncertainties for the charged pion, kaon, and (anti)proton spectra and for the particle ratios. Note that $K/\pi = (K^+ + K^-)/(\pi^+ + \pi^-)$ and $p/\pi = (p + \bar{p})/(\pi^+ + \pi^-)$.

used to constrain the fits. The uncertainty is calculated by varying the $\langle dE/dx \rangle$ and $\sigma_{dE/dx}$ in the particle fraction fits (Fig. 5) within the precision of the dE/dx response calibration, $\sim$1% and 5% for $\langle dE/dx \rangle$ and $\sigma_{dE/dx}$, respectively. A small fraction of this uncertainty was found to be multiplicity dependent, it was estimated as done in the previous ALICE publication [30].

A summary of the main systematic uncertainties on the p_T spectra and the particle ratios for p–Pb and pp collisions can be found in Table 3 for two p_T intervals. For pions, the main contribution is related to event and track selection and the associated common corrections. In the case of kaons and protons the largest uncertainty is attributed to the parametrization of the dE/dx response. For kaons, the uncertainty decreases with p_T and increases with multiplicity while for protons the multiplicity dependence is opposite. This variation mainly reflects the changes in the particle ratios with p_T and multiplicity.

5 Results and discussions

The total systematic uncertainty for all the spectra for a given particle species is factorized for each p_T interval into a multiplicity independent and multiplicity dependent systematic uncertainty. The transverse momentum distributions obtained from the different analyses are combined in the overlapping p_T region using a weighted average. The weight for the combinations was done according to the total systematic uncertainty to obtain the best overall precision. Since the systematic uncertainties due to normalization

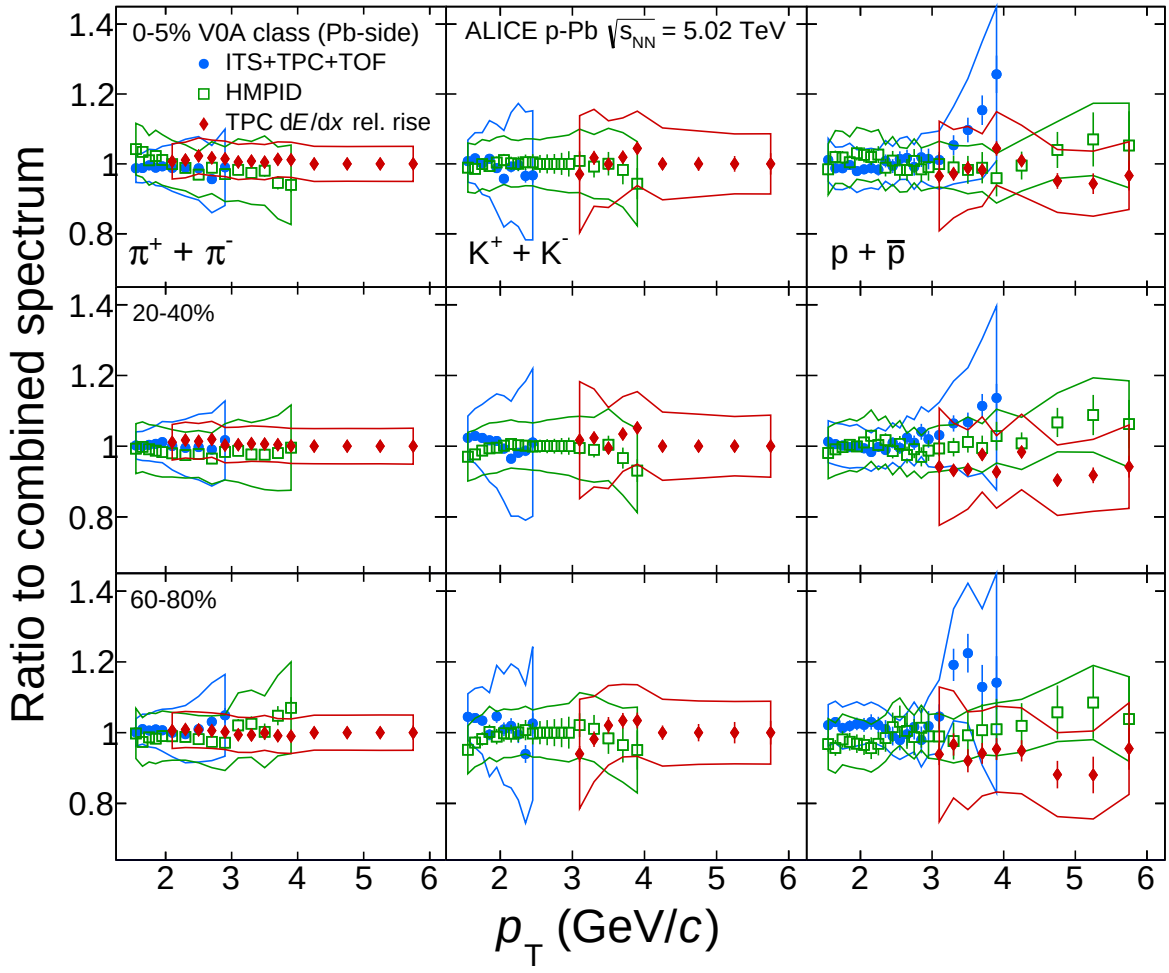

Fig. 6: (Color online.) The ratio of individual spectra to the combined spectrum as a function of p_{T} for pions (left), kaons (middle), and protons (right). From top-to-bottom the rows show the V0A multiplicity class 0–5%, 20–40% and 60–80%. Statistical and uncorrelated systematic uncertainties are shown as vertical error bars and error bands, respectively. Only the p_{T} ranges where individual analysis overlap are shown. See the text for further details.

and tracking are common to all the analyses, they were added directly to the final combined results. The statistical uncertainties are much smaller and therefore neglected in the combination weights. The multiplicity dependent systematic uncertainty for the combined spectra is also propagated using the same weights. For the results shown in this paper the full systematic uncertainty is always used, but the multiplicity correlated and uncorrelated systematic uncertainties are made available at HepData. Figure 6 shows examples of the comparisons among the individual analyses and the combined p_{T} spectra, focusing on the overlapping p_{T} region. Within systematic and statistical uncertainties the new high-p_{T} results, measured with HMPID and TPC, agree with the published results [30]. Similar agreement is obtained for the p_{T} spectra in INEL pp collisions at 7 TeV [39].

5.1 Transverse momentum spectra and nuclear modification factor

The combined charged pion, kaon and (anti)proton p_{T} spectra in p–Pb collisions for different V0A multiplicity classes are shown in Fig. 7. As reported in [30], for p_{T} below 2–3 GeV/c the spectra behave like in Pb–Pb collisions, i.e., the p_{T} distributions become harder as the multiplicity increases and the change is most pronounced for protons and lambdas. In heavy-ion collisions this effect is commonly attributed to radial flow. For larger momenta, the spectra follow a power-law shape as expected from perturbative QCD.

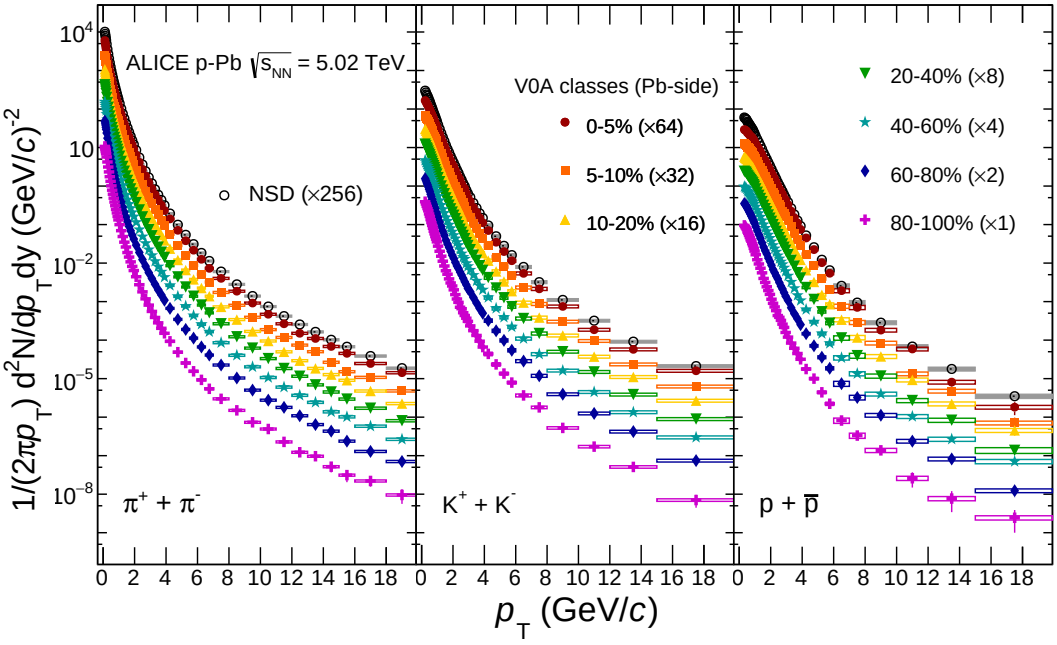

Fig. 7: (Color online.) Transverse momentum spectra of charged pions (left), kaons (middle), and (anti)protons (right) measured in p–Pb collisions at $\sqrt{s_{\rm NN}} = 5.02$ TeV. Statistical and systematic uncertainties are plotted as vertical error bars and boxes, respectively. The spectra (measured for NSD events and for different V0A multiplicity classes) have been scaled by the indicated factors in the legend for better visibility.

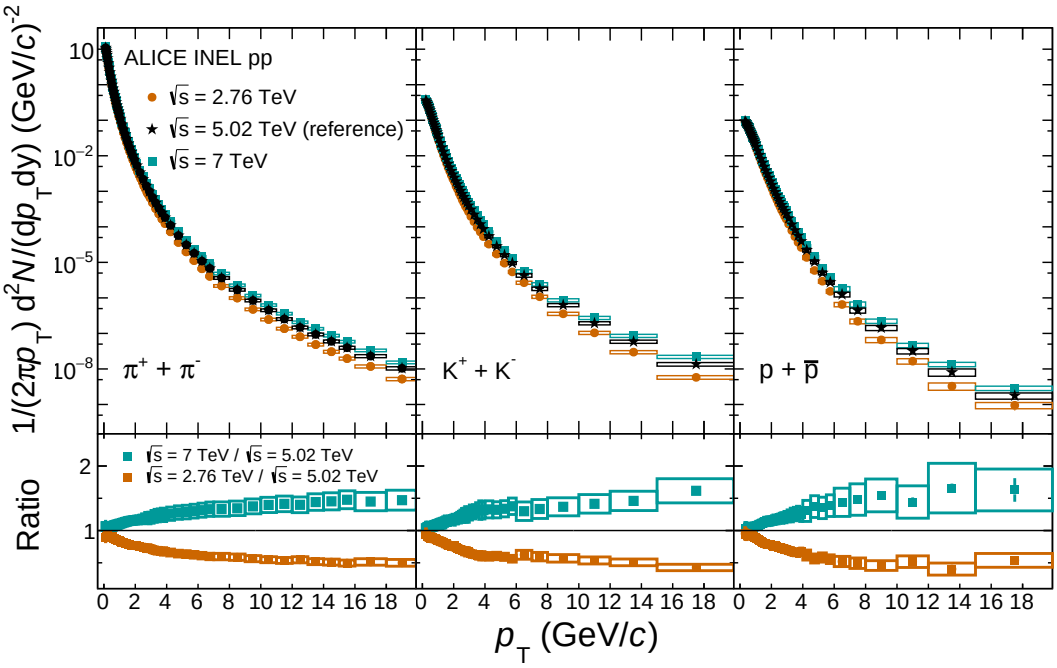

Fig. 8: (Color online.) Transverse momentum spectra of charged pions (left), kaons (middle), and (anti)protons (right) measured in INEL pp collisions at $\sqrt{s} = 2.76$ TeV and at $\sqrt{s} = 7$ TeV. Statistical and systematic uncertainties are plotted as vertical error bars and boxes, respectively. The spectrum at $\sqrt{s} = 5.02$ TeV represents the reference in INEL pp collisions, constructed from measured spectra at $\sqrt{s} = 2.76$ TeV and at $\sqrt{s} = 7$ TeV. See the text for further details. Panels on the bottom show the ratio of the measured yields to the interpolated spectra. Only uncertainties of the interpolated spectra are shown.

In order to quantify any particle species dependence of the nuclear effects in p–Pb collisions, comparisons to reference $p_{\rm T}$ spectra in pp collisions are needed. In the absence of pp data at $\sqrt{s} = 5.02$ TeV, the reference spectra are obtained by interpolating data measured at $\sqrt{s} = 2.76$ TeV and at $\sqrt{s} = 7$ TeV. The invariant cross section for identified hadron production in INEL pp collisions, $1/(2\pi p_{\rm T})\, {\rm d}^2\sigma_{\rm pp}^{\rm INEL}/{\rm d}y{\rm d}p_{\rm T}$, is interpolated in each $p_{\rm T}$ interval, assuming a power law dependence as a function of $\sqrt{s}$. The method was cross-checked using events simulated by Pythia 8.201 [55], where the difference between the interpolated and the simulated reference was found to be negligible. The maximum relative systematic uncertainty of the spectra at $\sqrt{s} = 2.76$ TeV and at $\sqrt{s} = 7$ TeV has been assigned as a systematic uncertainty to the reference. In the transverse momentum interval $3 < p_{\rm T} < 10$ GeV/c, the total systematic uncertainties for pions and kaons are below 8.6% and 10%, respectively. While for (anti)protons it is 7.7% and 18% at 3 GeV/c and 10 GeV/c, respectively. The invariant yields are shown in Fig. 8, where the interpolated $p_{\rm T}$ spectra are compared to those measured in INEL pp collisions at 2.76 TeV and 7 TeV.

The nuclear modification factor is then constructed as:

$$R_{\rm pPb} = \frac{{\rm d}^2N_{\rm pPb}/{\rm d}y{\rm d}p_{\rm T}}{\langle T_{\rm pPb}\rangle\, {\rm d}^2\sigma_{\rm pp}^{\rm INEL}/{\rm d}y{\rm d}p_{\rm T}} \tag{3}$$

where, for minimum bias (NSD) p–Pb collisions the average nuclear overlap function, $\langle T_{\rm pPb}\rangle$, is $0.0983 \pm 0.0035\ {\rm mb}^{-1}$ [43]. In absence of nuclear effects the $R_{\rm pPb}$ is expected to be one.

Figure 9 shows the identified hadron $R_{\rm pPb}$ compared to that for inclusive charged particles ($\rm h^{\pm}$) [54] in NSD p–Pb events. At high $p_{\rm T}$ (> 10 GeV/c), all nuclear modification factors are consistent with unity within systematic and statistical uncertainties. Around 4 GeV/c, where a prominent Cronin enhancement has been seen at lower energies [33, 34], the unidentified charged hadron $R_{\rm pPb}$ is above unity, albeit barely significant within systematic uncertainties [54]. Remarkably, the (anti)proton enhancement is $\sim$3 times larger than that for charged particles, while for charged pions and kaons the enhancement is below that of charged particles. The STAR and PHENIX Collaborations have observed a similar pattern at RHIC, where the nuclear modification factor for MB d-Au collisions, $R_{\rm dAu}$, in the range $2 < p_{\rm T} < 5$ GeV/c, is 1.24 ± 0.13 and 1.49 ± 0.17 for charged pions and (anti)protons, respectively [20].

An enhancement of protons in the same $p_{\rm T}$ range is also observed in heavy-ion collisions [35, 47], where it commonly is interpreted as radial-flow and has a strong centrality dependence. In the next section, we study the multiplicity dependence of the invariant yield ratios to see whether protons are more enhanced as a function of multiplicity than pions.

5.2 Transverse momentum and multiplicity dependence of particle ratios

The kaon-to-pion and the proton-to-pion ratios as a function of $p_{\rm T}$ for different V0A multiplicity classes are shown in Fig. 10. The results for p–Pb collisions are compared to those measured for INEL pp collisions at 2.76 TeV [35] and at 7 TeV [39]. Within systematic and statistical uncertainties, the $p_{\rm T}$ differential kaon-to-pion ratios do not show any multiplicity dependence. In fact, the results are similar to those for INEL pp collisions at both energies. The $p_{\rm T}$ differential proton-to-pion ratios show a clear multiplicity evolution at low and intermediate $p_{\rm T}$ (< 10 GeV/c). This multiplicity evolution is qualitatively similar to the centrality evolution observed in Pb–Pb collisions [35, 47].

It is worth noting that the average multiplicities at mid-rapidity for peripheral Pb–Pb collisions (60–80%) and high multiplicity p–Pb collisions (0–5% V0A multiplicity class) are very similar, $\langle {\rm d}N_{\rm ch}/{\rm d}\eta\rangle \sim 50$. Even if the physical mechanisms for particle production could be different, it seems interesting to compare these systems with similar underlying activity as done in Fig. 11, where INEL $\sqrt{s} = 7$ TeV pp results are included as an approximate baseline. Within systematic and statistical uncertainties, the kaon-to-pion ratios are the same for all systems. On the other hand, the proton-to-pion ratios exhibit similar flow-like features for the p–Pb and Pb–Pb systems, namely, the ratios are below the pp baseline for $p_{\rm T} < 1$ GeV/c

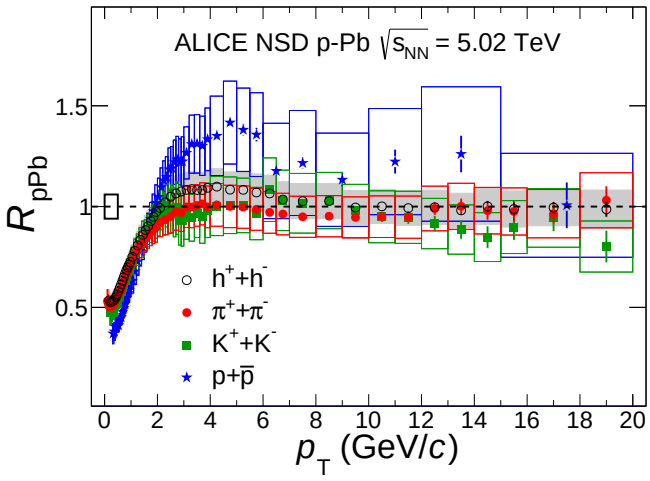

Fig. 9: (Color online.) The nuclear modification factor $R_{\rm pPb}$ as a function of transverse momentum $p_{\rm T}$ for different particle species. The statistical and systematic uncertainties are shown as vertical error bars and boxes, respectively. The total normalization uncertainty is indicated by a vertical scale of the empty box at $p_{\rm T} = 0\,\text{GeV}/c$ and $R_{\rm pPb} = 1$. The result for inclusive charged hadrons [54] is also shown.

and above for $p_{\rm T} > 1.5\,\text{GeV}/c$. Quantitative differences are observed between p–Pb and Pb–Pb results, but they can be attributed to the differences in the initial state overlap geometry and the beam energy.

The results for the particle ratios suggest that the modification of the (anti)proton spectral shape going from pp to p–Pb collisions could play the dominant role in the Cronin enhancement observed for inclusive charged particle $R_{\rm pPb}$ at LHC energies. To confirm this picture one would have to study the nuclear modification factor as a function of multiplicity as we did in [45], where, the possible biases in the evaluation of the multiplicity-dependent average nuclear overlap function $\langle T_{\rm pPb} \rangle$ were discussed. These results will become available in the future.

In Fig. 12 we compare the particle ratios at high $p_{\rm T}$ ($10 < p_{\rm T} < 20\,\text{GeV}/c$) measured in INEL $\sqrt{s} = 7$ TeV pp collisions, peripheral Pb–Pb collisions and the multiplicity dependent results in p–Pb collisions. Within statistical and systematic uncertainties, the ratios do not show any evolution with multiplicity. Moreover, since it has been already reported that in Pb–Pb collisions they are centrality independent [47] we conclude that they are system-size independent.

The strong similarity of particle ratios as a function of multiplicity in p–Pb and centrality in Pb–Pb collisions in the low, intermediate, and high-$p_{\rm T}$ regions is striking. In general, the results for p–Pb collisions appear to raise questions about the long standing ideas of specific physics models for small and large systems [56]. For example, in the low $p_{\rm T}$ publication [30], hydrodynamic inspired fits gave higher transverse expansion velocities ($\langle \beta_{\rm T} \rangle$) for p–Pb than for Pb–Pb collisions. Hydrodynamics, which successfully describes many features of heavy-ion collisions, has been applied to small systems and can explain this effect [21], but care needs to be taken since its applicability to small systems is still under debate [56]. On the other hand, models like color reconnection, where the soft and hard components are allowed to interact, produce this kind of effects in pp collisions [29, 57]. Even more, the hard collisions which could be enhanced via the multiplicity selection in small systems, also contribute to increase $\langle \beta_{\rm T} \rangle$ [58]. In general, color reconnection effects in p–Pb and Pb–Pb collisions are under investigation and models for the effect of strong color fields in small systems are in general under development [59]. Finally, it has been proposed that in d-Au collisions the recombination of soft and shower partons in the final state could explain the behavior of the nuclear modification factor at intermediate $p_{\rm T}$ [32]. The CMS Collaboration has found that the second-order (v_2) and the third-order (v_3) anisotropy harmonics

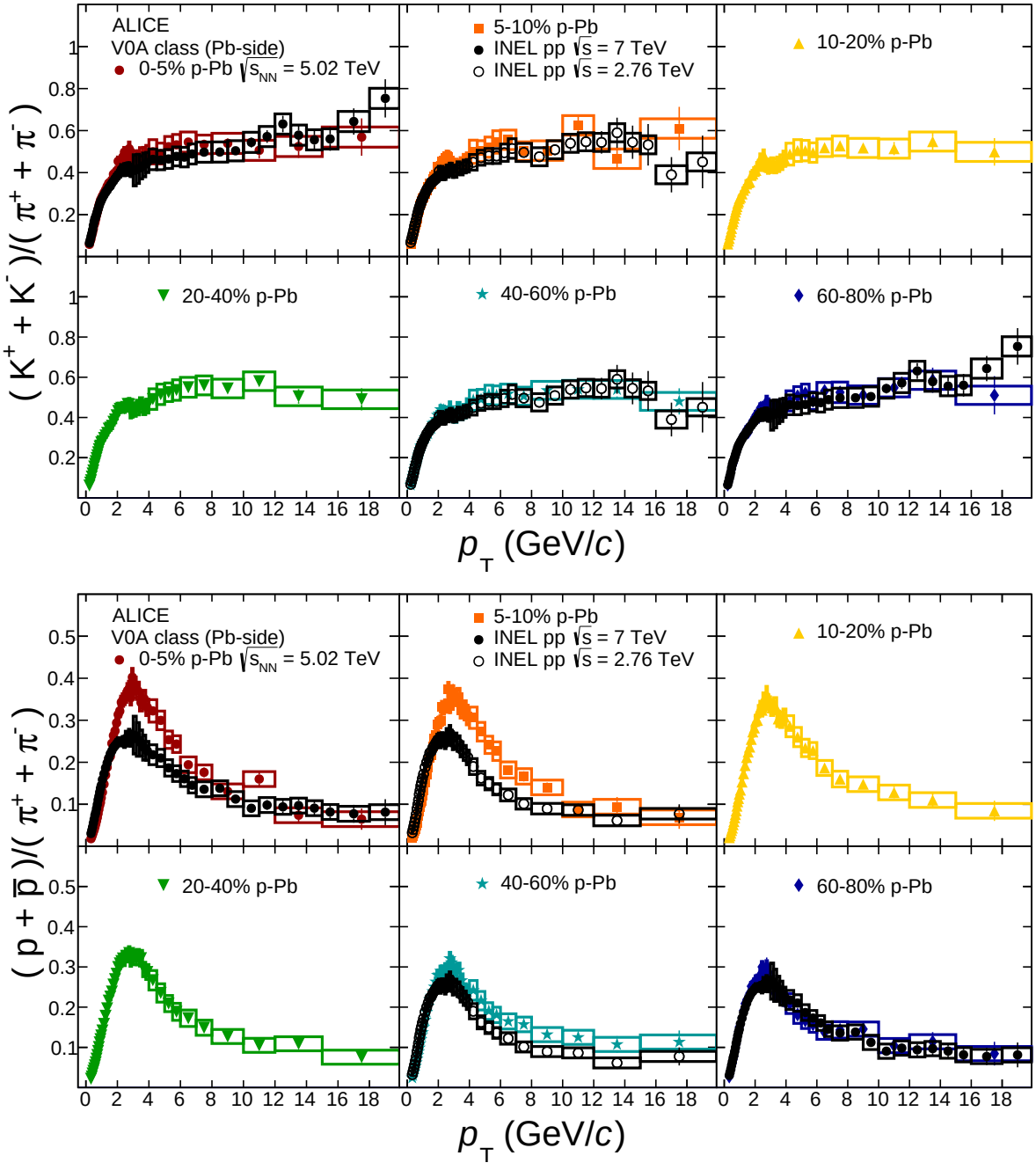

Fig. 10: (Color online.) Kaon-to-pion (upper panel) and proton-to-pion (bottom panel) ratios as a function of p_{T} for different V0A multiplicity classes. Results for p–Pb collisions (full markers) are compared to the ratios measured in INEL pp collisions at 2.76 TeV [35] (empty circles) and at 7 TeV [39] (full circles). The statistical and systematic uncertainties are plotted as vertical error bars and boxes, respectively.

measured for $\mathrm{K}^0_{\mathrm{S}}$ and Λ show constituent quark scaling in p–Pb collisions [60].

6 Conclusions

We have reported on the charged pion, kaon and (anti)proton production up to large transverse momenta ($p_{\mathrm{T}} \leq 20\,\mathrm{GeV}/c$) in p–Pb collisions at $\sqrt{s_{\mathrm{NN}}}$ =5.02 TeV. The p_{T} spectra in $\sqrt{s} = 7$ TeV pp collisions were also measured up to 20 GeV/c to allow the determination of the $\sqrt{s} = 5.02$ TeV pp reference cross

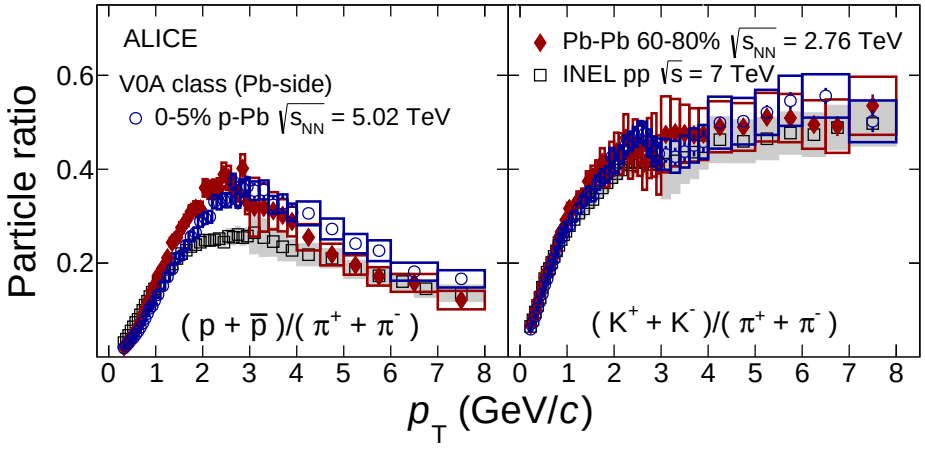

Fig. 11: (Color online.) Particle ratios as a function of transverse momentum. Three different colliding systems are compared, pp (open squares), 0–5% p–Pb (open circles) and 60–80% Pb–Pb (full diamonds) collisions at $\sqrt{s_{\rm NN}}$ = 7 TeV, 5.02 TeV and 2.76 TeV, respectively.

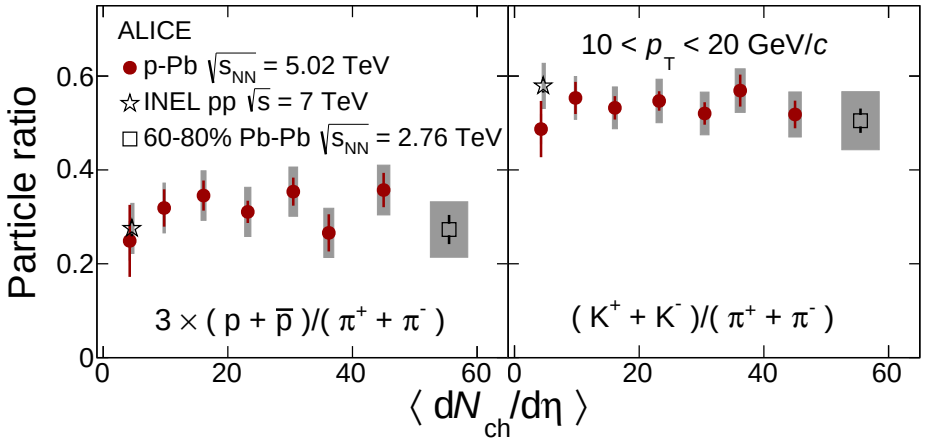

Fig. 12: (Color online.) Particle ratios as a function of $\langle {\rm d}N_{\rm ch}/{\rm d}\eta \rangle$ in each V0A multiplicity class (see [30] for more details). Three different colliding systems are compared: pp, p–Pb and peripheral Pb–Pb collisions.

section using the existing data at 2.76 TeV and at 7 TeV.

At intermediate $p_{\rm T}$ ($2 < p_{\rm T} < 10$ GeV/c), the (anti)proton $R_{\rm pPb}$ for non-single diffractive p–Pb collisions was found to be significantly larger than those for pions and kaons, in particular in the region where the Cronin peak was observed by experiments at lower energies. Hence, the modest enhancement which we already reported for unidentified charged particles can be attributed to the modification of the proton spectral shape going from pp to p–Pb collisions. At high $p_{\rm T}$ the nuclear modification factors for charged pions, kaons and (anti)protons are consistent with unity within systematic and statistical uncertainties.

The enhancement of protons with respect to pions at intermediate $p_{\rm T}$ shows a strong multiplicity dependence. This behavior is not observed for the kaon-to-pion ratio. At high transverse momenta ($10 < p_{\rm T} < 20$ GeV/c) the $p_{\rm T}$ integrated particle ratios are system-size independent for pp, p–Pb and Pb–Pb collisions. For a similar multiplicity at mid-rapidity, the $p_{\rm T}$-differential particle ratios are alike for p–Pb and Pb–Pb collisions over the broad $p_{\rm T}$ range reported in this paper.

Acknowledgements

The ALICE Collaboration would like to thank all its engineers and technicians for their invaluable contributions to the construction of the experiment and the CERN accelerator teams for the outstanding performance of the LHC complex. The ALICE Collaboration gratefully acknowledges the resources and support provided by all Grid centres and the Worldwide LHC Computing Grid (WLCG) collaboration. The ALICE Collaboration acknowledges the following funding agencies for their support in building and running the ALICE detector: State Committee of Science, World Federation of Scientists (WFS) and Swiss Fonds Kidagan, Armenia; Conselho Nacional de Desenvolvimento Científico e Tecnológico (CNPq), Financiadora de Estudos e Projetos (FINEP), Fundação de Amparo à Pesquisa do Estado de São Paulo (FAPESP); National Natural Science Foundation of China (NSFC), the Chinese Ministry of Education (CMOE) and the Ministry of Science and Technology of China (MSTC); Ministry of Education and Youth of the Czech Republic; Danish Natural Science Research Council, the Carlsberg Foundation and the Danish National Research Foundation; The European Research Council under the European Community's Seventh Framework Programme; Helsinki Institute of Physics and the Academy of Finland; French CNRS-IN2P3, the 'Region Pays de Loire', 'Region Alsace', 'Region Auvergne' and CEA, France; German Bundesministerium fur Bildung, Wissenschaft, Forschung und Technologie (BMBF) and the Helmholtz Association; General Secretariat for Research and Technology, Ministry of Development, Greece; National Research, Development and Innovation Office (NKFIH), Hungary; Department of Atomic Energy and Department of Science and Technology of the Government of India; Istituto Nazionale di Fisica Nucleare (INFN) and Centro Fermi - Museo Storico della Fisica e Centro Studi e Ricerche "Enrico Fermi", Italy; Japan Society for the Promotion of Science (JSPS) KAKENHI and MEXT, Japan; Joint Institute for Nuclear Research, Dubna; National Research Foundation of Korea (NRF); Consejo Nacional de Cienca y Tecnologia (CONACYT), Direccion General de Asuntos del Personal Academico(DGAPA), México, Amerique Latine Formation academique - European Commission (ALFA-EC) and the EPLANET Program (European Particle Physics Latin American Network); Stichting voor Fundamenteel Onderzoek der Materie (FOM) and the Nederlandse Organisatie voor Wetenschappelijk Onderzoek (NWO), Netherlands; Research Council of Norway (NFR); National Science Centre, Poland; Ministry of National Education/Institute for Atomic Physics and National Council of Scientific Research in Higher Education (CNCSI-UEFISCDI), Romania; Ministry of Education and Science of Russian Federation, Russian Academy of Sciences, Russian Federal Agency of Atomic Energy, Russian Federal Agency for Science and Innovations and The Russian Foundation for Basic Research; Ministry of Education of Slovakia; Department of Science and Technology, South Africa; Centro de Investigaciones Energeticas, Medioambientales y Tecnologicas (CIEMAT), E-Infrastructure shared between Europe and Latin America (EELA), Ministerio de Economía y Competitividad (MINECO) of Spain, Xunta de Galicia (Consellería de Educación), Centro de Aplicaciones Tecnolgicas y Desarrollo Nuclear (CEADEN), Cubaenergía, Cuba, and IAEA (International Atomic Energy Agency); Swedish Research Council (VR) and Knut & Alice Wallenberg Foundation (KAW); Ukraine Ministry of Education and Science; United Kingdom Science and Technology Facilities Council (STFC); The United States Department of Energy, the United States National Science Foundation, the State of Texas, and the State of Ohio; Ministry of Science, Education and Sports of Croatia and Unity through Knowledge Fund, Croatia; Council of Scientific and Industrial Research (CSIR), New Delhi, India; Pontificia Universidad Católica del Perú.

References

[1] **STAR** Collaboration, J. Adams *et al.*, "Experimental and theoretical challenges in the search for the quark gluon plasma: The STAR Collaboration's critical assessment of the evidence from RHIC collisions," *Nucl. Phys.* **A757** (2005) 102–183, arXiv:nucl-ex/0501009 [nucl-ex].

[2] **PHENIX** Collaboration, K. Adcox *et al.*, "Formation of dense partonic matter in relativistic

nucleus-nucleus collisions at RHIC: Experimental evaluation by the PHENIX collaboration," *Nucl. Phys.* **A757** (2005) 184–283, arXiv:nucl-ex/0410003 [nucl-ex].

[3] **BRAHMS** Collaboration, I. Arsene *et al.*, "Quark gluon plasma and color glass condensate at RHIC? The Perspective from the BRAHMS experiment," *Nucl. Phys.* **A757** (2005) 1–27, arXiv:nucl-ex/0410020 [nucl-ex].

[4] **PHOBOS** Collaboration, B. B. Back *et al.*, "The PHOBOS perspective on discoveries at RHIC," *Nucl. Phys.* **A757** (2005) 28–101, arXiv:nucl-ex/0410022 [nucl-ex].

[5] **ALICE** Collaboration, J. Schukraft, "Heavy Ion physics with the ALICE experiment at the CERN LHC," *Phil. Trans. Roy. Soc. Lond.* **A370** (2012) 917–932, arXiv:1109.4291 [hep-ex].

[6] **ALICE** Collaboration, K. Aamodt *et al.*, "Higher harmonic anisotropic flow measurements of charged particles in Pb-Pb collisions at $\sqrt{s_{\rm NN}}$=2.76 TeV," *Phys. Rev. Lett.* **107** (2011) 032301, arXiv:1105.3865 [nucl-ex].

[7] **ALICE** Collaboration, B. Abelev *et al.*, "Pion, Kaon, and Proton Production in Central Pb-Pb Collisions at $\sqrt{s_{\rm NN}} = 2.76$ TeV," *Phys. Rev. Lett.* **109** (2012) 252301, arXiv:1208.1974 [hep-ex].

[8] **ALICE** Collaboration, B. Abelev *et al.*, "Centrality Dependence of Charged Particle Production at Large Transverse Momentum in Pb-Pb Collisions at $\sqrt{s_{\rm NN}} = 2.76$ TeV," *Phys. Lett.* **B720** (2013) 52–62, arXiv:1208.2711 [hep-ex].

[9] **CMS** Collaboration, S. Chatrchyan *et al.*, "Study of high-pT charged particle suppression in PbPb compared to *pp* collisions at $\sqrt{s_{\rm NN}} = 2.76$ TeV," *Eur. Phys. J.* **C72** (2012) 1945, arXiv:1202.2554 [nucl-ex].

[10] **ALICE** Collaboration, B. Abelev *et al.*, "Measurement of charged jet suppression in Pb-Pb collisions at $\sqrt{s_{\rm NN}}$ = 2.76 TeV," *JHEP* **03** (2014) 013, arXiv:1311.0633 [nucl-ex].

[11] **ALICE** Collaboration, B. Abelev *et al.*, "Transverse sphericity of primary charged particles in minimum bias proton-proton collisions at $\sqrt{s} = 0.9$, 2.76 and 7 TeV," *Eur. Phys. J.* **C72** (2012) 2124, arXiv:1205.3963 [hep-ex].

[12] **CMS** Collaboration, S. Chatrchyan *et al.*, "Study of the production of charged pions, kaons, and protons in p-Pb collisions at $\sqrt{s_{\rm NN}} =$ 5.02 TeV," *Eur. Phys. J.* **C74** no. 6, (2014) 2847, arXiv:1307.3442 [hep-ex].

[13] **CMS** Collaboration, V. Khachatryan *et al.*, "Observation of long-range near-side angular correlations in proton-proton collisions at the LHC," *JHEP* **1009** (2010) 091, arXiv:1009.4122 [hep-ex].

[14] **CMS** Collaboration, S. Chatrchyan *et al.*, "Observation of long-range near-side angular correlations in proton-lead collisions at the LHC," *Phys. Lett.* **B718** (2013) 795–814, arXiv:1210.5482 [nucl-ex].

[15] **ALICE** Collaboration, B. Abelev *et al.*, "Long-range angular correlations on the near and away side in p-Pb collisions at $\sqrt{s_{\rm NN}} = 5.02$ TeV," *Phys. Lett.* **B719** (2013) 29–41, arXiv:1212.2001 [nucl-ex].

[16] **ATLAS** Collaboration, G. Aad *et al.*, "Observation of associated near-side and away-side long-range correlations in $\sqrt{s_{\rm NN}} = 5.02$TeV proton-lead collisions with the ATLAS detector," *Phys. Rev. Lett.* **110** no. **18**, (2013) 182302, arXiv:1212.5198 [hep-ex].

[17] **ATLAS** Collaboration, G. Aad *et al.*, "Measurement with the ATLAS detector of multi-particle azimuthal correlations in p-Pb collisions at $\sqrt{s_{\rm NN}} = 5.02$ TeV," *Phys. Lett.* **B725** (2013) 60–78, arXiv:1303.2084 [hep-ex].

[18] **CMS** Collaboration, S. Chatrchyan *et al.*, "Multiplicity and transverse momentum dependence of two- and four-particle correlations in p-Pb and Pb-Pb collisions," *Phys. Lett.* **B724** (2013) 213–240, arXiv:1305.0609 [nucl-ex].

[19] **PHENIX** Collaboration, A. Adare, S. Afansaiev, *et al.*, "Spectra and ratios of identified particles in Au+Au and d+Au collisions at $\sqrt{s_{\rm NN}} = 200$ GeV," *Phys. Rev.* **C88** (Aug, 2013) 024906. http://link.aps.org/doi/10.1103/PhysRevC.88.024906.

[20] **STAR** Collaboration, J. Adams *et al.*, "Identified hadron spectra at large transverse momentum in p+p and d+Au collisions at 200 GeV," *Phys. Lett.* **B637** (2006) 161–169, arXiv:nucl-ex/0601033 [nucl-ex].

[21] E. Shuryak and I. Zahed, "High-multiplicity pp and pA collisions: Hydrodynamics at its edge," *Phys. Rev. C* **88** no. 4, (2013) 044915, arXiv:1301.4470 [hep-ph].

[22] K. Werner, M. Bleicher, B. Guiot, I. Karpenko, and T. Pierog, "Evidence for Flow from Hydrodynamic Simulations of p-Pb Collisions at 5.02 TeV from v_2 Mass Splitting," *Phys. Rev. Lett.* **112** no. 23, (2014) 232301, arXiv:1307.4379 [nucl-th].

[23] P. Bozek, W. Broniowski, and G. Torrieri, "Mass hierarchy in identified particle distributions in proton-lead collisions," *Phys. Rev. Lett.* **111** (2013) 172303, arXiv:1307.5060 [nucl-th].

[24] A. Dumitru, K. Dusling, F. Gelis, J. Jalilian-Marian, T. Lappi, *et al.*, "The Ridge in proton-proton collisions at the LHC," *Phys. Lett.* **B697** (2011) 21–25.

[25] B. Schenke, S. Schlichting, and R. Venugopalan, "Azimuthal anisotropies in p-Pb collisions from classical Yang-Mills dynamics," *Phys. Lett.* **B747** (2015) 76–82, arXiv:1502.01331 [hep-ph].

[26] G.-L. Ma and A. Bzdak, "Long-range azimuthal correlations in proton-proton and proton-nucleus collisions from the incoherent scattering of partons," *Phys. Lett.* **B739** 209–213, arXiv:1404.4129 [hep-ph].

[27] T. Sjöstrand, S. Mrenna, and P. Z. Skands, "A Brief Introduction to PYTHIA 8.1," *Comput. Phys. Commun.* **178** (2008) 852–867.

[28] R. Corke and T. Sjöstrand, "Interleaved Parton Showers and Tuning Prospects," *JHEP* **03** (2011) 032, arXiv:1011.1759 [hep-ph].

[29] A. Ortiz, P. Christiansen, E. Cuautle, I. A. Maldonado, and G. Paić, "Color reconnection and flowlike patterns in pp collisions," *Phys. Rev. Lett.* **111** (Jul, 2013) 042001. http://link.aps.org/doi/10.1103/PhysRevLett.111.042001.

[30] **ALICE** Collaboration, B. B. Abelev *et al.*, "Multiplicity dependence of pion, kaon, proton and lambda production in p-Pb Collisions at $\sqrt{s_{\rm NN}} = 5.02$ TeV," *Phys. Lett.* **B728** (2014) 25–38, arXiv:1307.6796 [nucl-ex].

[31] B. Kopeliovich, J. Nemchik, A. Schafer, and A. Tarasov, "Cronin effect in hadron production off nuclei," *Phys. Rev. Lett.* **88** (2002) 232303, arXiv:hep-ph/0201010 [hep-ph].

[32] R. C. Hwa and C. B. Yang, "Final state interaction as the origin of the Cronin effect," *Phys. Rev. Lett.* **93** (2004) 082302, arXiv:nucl-th/0403001 [nucl-th].

[33] J. W. Cronin, H. J. Frisch, M. J. Shochet, J. P. Boymond, P. A. Piroué, and R. L. Sumner, "Production of Hadrons with Large Transverse Momentum at 200-GeV and 300-GeV.," *Phys. Rev. Lett.* **31** (Dec, 1973) 1426–1429.

[34] J. W. Cronin, H. J. Frisch, M. J. Shochet, J. P. Boymond, P. A. Piroué, and R. L. Sumner, "Production of hadrons at large transverse momentum at 200, 300, and 400 gev," *Phys. Rev.* **D11** (Jun, 1975) 3105–3123. http://link.aps.org/doi/10.1103/PhysRevD.11.3105.

[35] **ALICE** Collaboration, B. B. Abelev *et al.*, "Production of charged pions, kaons and protons at large transverse momenta in pp and Pb-Pb collisions at $\sqrt{s_{\rm NN}}$ =2.76 TeV," *Phys. Lett.* **B736** (2014) 196–207, arXiv:1401.1250 [nucl-ex].

[36] P. Huovinen, P. F. Kolb, U. W. Heinz, P. V. Ruuskanen, and S. A. Voloshin, "Radial and elliptic flow at RHIC: Further predictions," *Phys. Lett.* **B503** (2001) 58–64, arXiv:hep-ph/0101136 [hep-ph].

[37] K. P. Das and R. C. Hwa, "Quark - anti-Quark Recombination in the Fragmentation Region," *Phys. Lett.* **B68** (1977) 459. [Erratum: Phys. Lett.73B,504(1978)].

[38] N. Armesto, H. Paukkunen, J. M. Penn, C. A. Salgado, and P. Zurita, "An analysis of the impact of LHC Run I proton-lead data on nuclear parton densities," *Eur. Phys. J.* **C76** no. 4, (2016) 218, arXiv:1512.01528 [hep-ph].

[39] **ALICE** Collaboration, J. Adam *et al.*, "Measurement of pion, kaon and proton production in proton-proton collisions at $\sqrt{s} = 7$ TeV," *Eur. Phys. J.* **C75** no. 5, (2015) 226, arXiv:1504.00024 [nucl-ex].

[40] **ALICE** Collaboration, B. B. Abelev *et al.*, "Energy dependence of the transverse momentum distributions of charged particles in pp collisions Measured by ALICE," *Eur. Phys. J.* **C73** no. 12, (2013) 2662, arXiv:1307.1093 [nucl-ex].

[41] **ALICE** Collaboration, K. Aamodt *et al.*, "The ALICE experiment at the CERN LHC," *JINST* **3** (2008) S08002.

[42] **ALICE** Collaboration, B. B. Abelev *et al.*, "Performance of the ALICE Experiment at the CERN LHC," *Int. J. Mod. Phys.* **A29** (2014) 1430044, arXiv:1402.4476 [nucl-ex].

[43] **ALICE** Collaboration, B. Abelev *et al.*, "Transverse momentum distribution and nuclear modification factor of charged particles in p-Pb collisions at $\sqrt{s_{\rm NN}} = 5.02$ TeV," *Phys. Rev. Lett.* **110** no. 8, (2013) 082302, arXiv:1210.4520 [nucl-ex].

[44] **ALICE** Collaboration, K. Aamodt *et al.*, "Performance of the alice vzero system," *J. of Inst.* **8** no. 10, (2013) P10016. http://stacks.iop.org/1748-0221/8/i=10/a=P10016.

[45] **ALICE** Collaboration, J. Adam *et al.*, "Centrality dependence of particle production in p-Pb collisions at $\sqrt{s_{\rm NN}}$= 5.02 TeV," *Phys. Rev.* **C91** no. 6, (2015) 064905, arXiv:1412.6828 [nucl-ex].

[46] **ALICE** Collaboration, B. Abelev *et al.*, "Pseudorapidity density of charged particles in p + Pb collisions at $\sqrt{s_{NN}} = 5.02$ TeV," *Phys. Rev. Lett.* **110** no. 3, (2013) 032301, arXiv:1210.3615 [nucl-ex].

[47] **ALICE** Collaboration, J. Adam *et al.*, "Centrality dependence of the nuclear modification factor of charged pions, kaons, and protons in Pb-Pb collisions at $\sqrt{s_{\rm NN}} = 2.76$ TeV," *Phys. Rev.* **C93** no. 3, (2016) 034913, arXiv:1506.07287 [nucl-ex].

[48] **ALICE** Collaboration, K. Aamodt *et al.*, "Production of pions, kaons and protons in pp collisions at $\sqrt{s} = 900$ GeV with ALICE at the LHC," *Eur. Phys. J.* **C71** (2011) 1655, arXiv:1101.4110 [hep-ex].

[49] **ALICE** Collaboration, F. Piuz, W. Klempt, L. Leistam, J. De Groot, and J. Schukraft, *ALICE high-momentum particle identification: Technical Design Report*. Technical Design Report ALICE. CERN, Geneva, 1998. https://cds.cern.ch/record/381431.

[50] **ALICE** Collaboration, J. Alme, Y. Andres, *et al.*, "The {ALICE} tpc, a large 3-dimensional tracking device with fast readout for ultra-high multiplicity events," *Nuclear Instruments and Methods in Physics Research Section A: Accelerators, Spectrometers, Detectors and Associated Equipment* **622** no. 1, (2010) 316 – 367. http://www.sciencedirect.com/science/article/pii/S0168900210008910.

[51] **ALICE** Collaboration, D. Di Bari, "The pattern recognition method for the CsI-RICH detector in ALICE," *Nucl. Instrum. Meth.* **A502** (2003) 300–304.

[52] S. Roesler, R. Engel, and J. Ranft, "The Monte Carlo event generator DPMJET-III," in *Advanced Monte Carlo for radiation physics, particle transport simulation and applications. Proceedings, Conference, MC2000, Lisbon, Portugal, October 23-26, 2000*, pp. 1033–1038. 2000. arXiv:hep-ph/0012252 [hep-ph]. http://www-public.slac.stanford.edu/sciDoc/docMeta.aspx?slacPubNumber=SLAC-PUB-8740.

[53] R. Engel, "Photoproduction within the two-component Dual Parton Model: amplitudes and cross sections," *Z. Phys.* **C66** (1995) 203–214.

[54] **ALICE** Collaboration, B. B. Abelev *et al.*, "Transverse momentum dependence of inclusive primary charged-particle production in p-Pb collisions at $\sqrt{s_{\rm NN}} = 5.02$ TeV," *Eur. Phys. J.* **C74** no. 9, (2014) 3054, arXiv:1405.2737 [nucl-ex].

[55] T. Sjöstrand, S. Ask, J. R. Christiansen, R. Corke, N. Desai, *et al.*, "An Introduction to PYTHIA 8.2," *Comput. Phys. Commun.* **191** (2015) 159–177, arXiv:1410.3012 [hep-ph].

[56] F. Antinori *et al.*, "Thoughts on opportunities from high-energy nuclear collisions," arXiv:1409.2981 [hep-ph].

[57] C. Bierlich and J. R. Christiansen, "Effects of Colour Reconnection on Hadron Flavour Observables," arXiv:1507.02091 [hep-ph].

[58] A. Ortiz, E. Cuautle, and G. Paić, "Mid-rapidity charged hadron transverse spherocity in pp collisions simulated with pythia," *Nucl. Phys.* **A941** no. 0, (2015) 78 – 86. http://www.sciencedirect.com/science/article/pii/S0375947415001311.

[59] C. Bierlich, G. Gustafson, L. Lönnblad, and A. Tarasov, "Effects of Overlapping Strings in pp Collisions," *JHEP* **1503** (2015) 148, arXiv:1412.6259 [hep-ph].

[60] **CMS** Collaboration, V. Khachatryan *et al.*, "Long-range two-particle correlations of strange hadrons with charged particles in pPb and PbPb collisions at LHC energies," *Phys. Lett. B* **742** (2015) 200–224, arXiv:1409.3392 [nucl-ex].

A The ALICE Collaboration

J. Adam[40] , D. Adamová[84] , M.M. Aggarwal[88] , G. Aglieri Rinella[36] , M. Agnello[110] , N. Agrawal[48] , Z. Ahammed[132] , S. Ahmad[19] , S.U. Ahn[68] , S. Aiola[136] , A. Akindinov[58] , S.N. Alam[132] , D. Aleksandrov[80] , B. Alessandro[110] , D. Alexandre[101] , R. Alfaro Molina[64] , A. Alici[12,104] , A. Alkin[3] , J.R.M. Almaraz[119] , J. Alme[38] , T. Alt[43] , S. Altinpinar[18] , I. Altsybeev[131] , C. Alves Garcia Prado[120] , C. Andrei[78] , A. Andronic[97] , V. Anguelov[94] , T. Antičić[98] , F. Antinori[107] , P. Antonioli[104] , L. Aphecetche[113] , H. Appelshäuser[53] , S. Arcelli[28] , R. Arnaldi[110] , O.W. Arnold[37,93] , I.C. Arsene[22] , M. Arslandok[53] , B. Audurier[113] , A. Augustinus[36] , R. Averbeck[97] , M.D. Azmi[19] , A. Badalà[106] , Y.W. Baek[67] , S. Bagnasco[110] , R. Bailhache[53] , R. Bala[91] , S. Balasubramanian[136] , A. Baldisseri[15] , R.C. Baral[61] , A.M. Barbano[27] , R. Barbera[29] , F. Barile[33] , G.G. Barnaföldi[135] , L.S. Barnby[101] , V. Barret[70] , P. Bartalini[7] , K. Barth[36] , J. Bartke[117] , E. Bartsch[53] , M. Basile[28] , N. Bastid[70] , S. Basu[132] , B. Bathen[54] , G. Batigne[113] , A. Batista Camejo[70] , B. Batyunya[66] , P.C. Batzing[22] , I.G. Bearden[81] , H. Beck[53] , C. Bedda[110] , N.K. Behera[50] , I. Belikov[55] , F. Bellini[28] , H. Bello Martinez[2] , R. Bellwied[122] , R. Belmont[134] , E. Belmont-Moreno[64] , V. Belyaev[75] , P. Benacek[84] , G. Bencedi[135] , S. Beole[27] , I. Berceanu[78] , A. Bercuci[78] , Y. Berdnikov[86] , D. Berenyi[135] , R.A. Bertens[57] , D. Berzano[36] , L. Betev[36] , A. Bhasin[91] , I.R. Bhat[91] , A.K. Bhati[88] , B. Bhattacharjee[45] , J. Bhom[128] , L. Bianchi[122] , N. Bianchi[72] , C. Bianchin[134,57] , J. Bielčík[40] , J. Bielčíková[84] , A. Bilandzic[81,37,93] , G. Biro[135] , R. Biswas[4] , S. Biswas[79] , S. Bjelogrlic[57] , J.T. Blair[118] , D. Blau[80] , C. Blume[53] , F. Bock[74,94] , A. Bogdanov[75] , H. Bøggild[81] , L. Boldizsár[135] , M. Bombara[41] , J. Book[53] , H. Borel[15] , A. Borissov[96] , M. Borri[83,124] , F. Bossú[65] , E. Botta[27] , C. Bourjau[81] , P. Braun-Munzinger[97] , M. Bregant[120] , T. Breitner[52] , T.A. Broker[53] , T.A. Browning[95] , M. Broz[40] , E.J. Brucken[46] , E. Bruna[110] , G.E. Bruno[33] , D. Budnikov[99] , H. Buesching[53] , S. Bufalino[36,27] , P. Buncic[36] , O. Busch[94,128] , Z. Buthelezi[65] , J.B. Butt[16] , J.T. Buxton[20] , D. Caffarri[36] , X. Cai[7] , H. Caines[136] , L. Calero Diaz[72] , A. Caliva[57] , E. Calvo Villar[102] , P. Camerini[26] , F. Carena[36] , W. Carena[36] , F. Carnesecchi[28] , J. Castillo Castellanos[15] , A.J. Castro[125] , E.A.R. Casula[25] , C. Ceballos Sanchez[9] , P. Cerello[110] , J. Cerkala[115] , B. Chang[123] , S. Chapeland[36] , M. Chartier[124] , J.L. Charvet[15] , S. Chattopadhyay[132] , S. Chattopadhyay[100] , A. Chauvin[93,37] , V. Chelnokov[3] , M. Cherney[87] , C. Cheshkov[130] , B. Cheynis[130] , V. Chibante Barroso[36] , D.D. Chinellato[121] , S. Cho[50] , P. Chochula[36] , K. Choi[96] , M. Chojnacki[81] , S. Choudhury[132] , P. Christakoglou[82] , C.H. Christensen[81] , P. Christiansen[34] , T. Chujo[128] , S.U. Chung[96] , C. Cicalo[105] , L. Cifarelli[12,28] , F. Cindolo[104] , J. Cleymans[90] , F. Colamaria[33] , D. Colella[59,36] , A. Collu[74,25] , M. Colocci[28] , G. Conesa Balbastre[71] , Z. Conesa del Valle[51] , M.E. Connors[ii,136] , J.G. Contreras[40] , T.M. Cormier[85] , Y. Corrales Morales[110] , I. Cortés Maldonado[2] , P. Cortese[32] , M.R. Cosentino[120] , F. Costa[36] , P. Crochet[70] , R. Cruz Albino[11] , E. Cuautle[63] , L. Cunqueiro[54,36] , T. Dahms[93,37] , A. Dainese[107] , M.C. Danisch[94] , A. Danu[62] , D. Das[100] , I. Das[100] , S. Das[4] , A. Dash[121,79] , S. Dash[48] , S. De[120] , A. De Caro[12,31] , G. de Cataldo[103] , C. de Conti[120] , J. de Cuveland[43] , A. De Falco[25] , D. De Gruttola[12,31] , N. De Marco[110] , S. De Pasquale[31] , A. Deisting[97,94] , A. Deloff[77] , E. Dénes[135,i], C. Deplano[82] , P. Dhankher[48] , D. Di Bari[33] , A. Di Mauro[36] , P. Di Nezza[72] , M.A. Diaz Corchero[10] , T. Dietel[90] , P. Dillenseger[53] , R. Divià[36] , Ø. Djuvsland[18] , A. Dobrin[62,82] , D. Domenicis Gimenez[120] , B. Dönigus[53] , O. Dordic[22] , T. Drozhzhova[53] , A.K. Dubey[132] , A. Dubla[57] , L. Ducroux[130] , P. Dupieux[70] , R.J. Ehlers[136] , D. Elia[103] , E. Endress[102] , H. Engel[52] , E. Epple[136] , B. Erazmus[113] , I. Erdemir[53] , F. Erhardt[129] , B. Espagnon[51] , M. Estienne[113] , S. Esumi[128] , J. Eum[96] , D. Evans[101] , S. Evdokimov[111] , G. Eyyubova[40] , L. Fabbietti[93,37] , D. Fabris[107] , J. Faivre[71] , A. Fantoni[72] , M. Fasel[74] , L. Feldkamp[54] , A. Feliciello[110] , G. Feofilov[131] , J. Ferencei[84] , A. Fernández Téllez[2] , E.G. Ferreiro[17] , A. Ferretti[27] , A. Festanti[30] , V.J.G. Feuillard[15,70] , J. Figiel[117] , M.A.S. Figueredo[124,120] , S. Filchagin[99] , D. Finogeev[56] , F.M. Fionda[25] , E.M. Fiore[33] , M.G. Fleck[94] , M. Floris[36] , S. Foertsch[65] , P. Foka[97] , S. Fokin[80] , E. Fragiacomo[109] , A. Francescon[36,30] , U. Frankenfeld[97] , G.G. Fronze[27] , U. Fuchs[36] , C. Furget[71] , A. Furs[56] , M. Fusco Girard[31] , J.J. Gaardhøje[81] , M. Gagliardi[27] , A.M. Gago[102] , M. Gallio[27] , D.R. Gangadharan[74] , P. Ganoti[89] , C. Gao[7] , C. Garabatos[97] , E. Garcia-Solis[13] , C. Gargiulo[36] , P. Gasik[93,37] , E.F. Gauger[118] , M. Germain[113] , A. Gheata[36] , M. Gheata[36,62] , P. Ghosh[132] , S.K. Ghosh[4] , P. Gianotti[72] , P. Giubellino[110,36] , P. Giubilato[30] , E. Gladysz-Dziadus[117] , P. Glässel[94] , D.M. Goméz Coral[64] , A. Gomez Ramirez[52] , V. Gonzalez[10] , P. González-Zamora[10] , S. Gorbunov[43] , L. Görlich[117] , S. Gotovac[116] , V. Grabski[64] , O.A. Grachov[136] , L.K. Graczykowski[133] , K.L. Graham[101] , A. Grelli[57] , A. Grigoras[36] , C. Grigoras[36] , V. Grigoriev[75] , A. Grigoryan[1] , S. Grigoryan[66] , B. Grinyov[3] , N. Grion[109] , J.M. Gronefeld[97] , J.F. Grosse-Oetringhaus[36] , J.-Y. Grossiord[130] , R. Grosso[97] , F. Guber[56] , R. Guernane[71] , B. Guerzoni[28] , K. Gulbrandsen[81] , T. Gunji[127] , A. Gupta[91] , R. Gupta[91] , R. Haake[54] , Ø. Haaland[18] , C. Hadjidakis[51] , M. Haiduc[62] , H. Hamagaki[127] , G. Hamar[135] , J.C. Hamon[55] , J.W. Harris[136] , A. Harton[13] , D. Hatzifotiadou[104] , S. Hayashi[127] , S.T. Heckel[53] , H. Helstrup[38] , A. Herghelegiu[78] , G. Herrera Corral[11] , B.A. Hess[35] , K.F. Hetland[38] , H. Hillemanns[36] , B. Hippolyte[55] , D. Horak[40] , R. Hosokawa[128] , P. Hristov[36] , M. Huang[18] , T.J. Humanic[20] , N. Hussain[45] , T. Hussain[19] , D. Hutter[43] , D.S. Hwang[21] , R. Ilkaev[99] , M. Inaba[128] , E. Incani[25] ,

M. Ippolitov[75,80], M. Irfan[19], M. Ivanov[97], V. Ivanov[86], V. Izucheev[111], N. Jacazio[28], P.M. Jacobs[74], M.B. Jadhav[48], S. Jadlovska[115], J. Jadlovsky[115,59], C. Jahnke[120], M.J. Jakubowska[133], H.J. Jang[68], M.A. Janik[133], P.H.S.Y. Jayarathna[122], C. Jena[30], S. Jena[122], R.T. Jimenez Bustamante[97], P.G. Jones[101], A. Jusko[101], P. Kalinak[59], A. Kalweit[36], J. Kamin[53], J.H. Kang[137], V. Kaplin[75], S. Kar[132], A. Karasu Uysal[69], O. Karavichev[56], T. Karavicheva[56], L. Karayan[97,94], E. Karpechev[56], U. Kebschull[52], R. Keidel[138], D.L.D. Keijdener[57], M. Keil[36], M. Mohisin Khan[iii,19], P. Khan[100], S.A. Khan[132], A. Khanzadeev[86], Y. Kharlov[111], B. Kileng[38], D.W. Kim[44], D.J. Kim[123], D. Kim[137], H. Kim[137], J.S. Kim[44], M. Kim[137], S. Kim[21], T. Kim[137], S. Kirsch[43], I. Kisel[43], S. Kiselev[58], A. Kisiel[133], G. Kiss[135], J.L. Klay[6], C. Klein[53], J. Klein[36], C. Klein-Bösing[54], S. Klewin[94], A. Kluge[36], M.L. Knichel[94], A.G. Knospe[118,122], C. Kobdaj[114], M. Kofarago[36], T. Kollegger[97], A. Kolojvari[131], V. Kondratiev[131], N. Kondratyeva[75], E. Kondratyuk[111], A. Konevskikh[56], M. Kopcik[115], P. Kostarakis[89], M. Kour[91], C. Kouzinopoulos[36], O. Kovalenko[77], V. Kovalenko[131], M. Kowalski[117], G. Koyithatta Meethaleveedu[48], I. Králik[59], A. Kravčáková[41], M. Kretz[43], M. Krivda[59,101], F. Krizek[84], E. Kryshen[86,36], M. Krzewicki[43], A.M. Kubera[20], V. Kučera[84], C. Kuhn[55], P.G. Kuijer[82], A. Kumar[91], J. Kumar[48], L. Kumar[88], S. Kumar[48], P. Kurashvili[77], A. Kurepin[56], A.B. Kurepin[56], A. Kuryakin[99], M.J. Kweon[50], Y. Kwon[137], S.L. La Pointe[110], P. La Rocca[29], P. Ladron de Guevara[11], C. Lagana Fernandes[120], I. Lakomov[36], R. Langoy[42], C. Lara[52], A. Lardeux[15], A. Lattuca[27], E. Laudi[36], R. Lea[26], L. Leardini[94], G.R. Lee[101], S. Lee[137], F. Lehas[82], R.C. Lemmon[83], V. Lenti[103], E. Leogrande[57], I. León Monzón[119], H. León Vargas[64], M. Leoncino[27], P. Lévai[135], S. Li[7,70], X. Li[14], J. Lien[42], R. Lietava[101], S. Lindal[22], V. Lindenstruth[43], C. Lippmann[97], M.A. Lisa[20], H.M. Ljunggren[34], D.F. Lodato[57], P.I. Loenne[18], V. Loginov[75], C. Loizides[74], X. Lopez[70], E. López Torres[9], A. Lowe[135], P. Luettig[53], M. Lunardon[30], G. Luparello[26], T.H. Lutz[136], A. Maevskaya[56], M. Mager[36], S. Mahajan[91], S.M. Mahmood[22], A. Maire[55], R.D. Majka[136], M. Malaev[86], I. Maldonado Cervantes[63], L. Malinina[iv,66], D. Mal'Kevich[58], P. Malzacher[97], A. Mamonov[99], V. Manko[80], F. Manso[70], V. Manzari[103,36], M. Marchisone[65,126,27], J. Mareš[60], G.V. Margagliotti[26], A. Margotti[104], J. Margutti[57], A. Marín[97], C. Markert[118], M. Marquard[53], N.A. Martin[97], J. Martin Blanco[113], P. Martinengo[36], M.I. Martínez[2], G. Martínez García[113], M. Martinez Pedreira[36], A. Mas[120], S. Masciocchi[97], M. Masera[27], A. Masoni[105], L. Massacrier[113], A. Mastroserio[33], A. Matyja[117], C. Mayer[117,36], J. Mazer[125], M.A. Mazzoni[108], D. Mcdonald[122], F. Meddi[24], Y. Melikyan[75], A. Menchaca-Rocha[64], E. Meninno[31], J. Mercado Pérez[94], M. Meres[39], Y. Miake[128], M.M. Mieskolainen[46], K. Mikhaylov[66,58], L. Milano[74,36], J. Milosevic[22], L.M. Minervini[103,23], A. Mischke[57], A.N. Mishra[49], D. Miśkowiec[97], J. Mitra[132], C.M. Mitu[62], N. Mohammadi[57], B. Mohanty[79,132], L. Molnar[55,113], L. Montaño Zetina[11], E. Montes[10], D.A. Moreira De Godoy[113,54], L.A.P. Moreno[2], S. Moretto[30], A. Morreale[113], A. Morsch[36], V. Muccifora[72], E. Mudnic[116], D. Mühlheim[54], S. Muhuri[132], M. Mukherjee[132], J.D. Mulligan[136], M.G. Munhoz[120], R.H. Munzer[93,37], H. Murakami[127], S. Murray[65], L. Musa[36], J. Musinsky[59], B. Naik[48], R. Nair[77], B.K. Nandi[48], R. Nania[104], E. Nappi[103], M.U. Naru[16], H. Natal da Luz[120], C. Nattrass[125], S.R. Navarro[2], K. Nayak[79], R. Nayak[48], T.K. Nayak[132], S. Nazarenko[99], A. Nedosekin[58], L. Nellen[63], F. Ng[122], M. Nicassio[97], M. Niculescu[62], J. Niedziela[36], B.S. Nielsen[81], S. Nikolaev[80], S. Nikulin[80], V. Nikulin[86], F. Noferini[104,12], P. Nomokonov[66], G. Nooren[57], J.C.C. Noris[2], J. Norman[124], A. Nyanin[80], J. Nystrand[18], H. Oeschler[94], S. Oh[136], S.K. Oh[67], A. Ohlson[36], A. Okatan[69], T. Okubo[47], L. Olah[135], J. Oleniacz[133], A.C. Oliveira Da Silva[120], M.H. Oliver[136], J. Onderwaater[97], C. Oppedisano[110], R. Orava[46], A. Ortiz Velasquez[63], A. Oskarsson[34], J. Otwinowski[117], K. Oyama[94,76], M. Ozdemir[53], Y. Pachmayer[94], P. Pagano[31], G. Paić[63], S.K. Pal[132], J. Pan[134], A.K. Pandey[48], V. Papikyan[1], G.S. Pappalardo[106], P. Pareek[49], W.J. Park[97], S. Parmar[88], A. Passfeld[54], V. Paticchio[103], R.N. Patra[132], B. Paul[100], H. Pei[7], T. Peitzmann[57], H. Pereira Da Costa[15], D. Peresunko[80,75], C.E. Pérez Lara[82], E. Perez Lezama[53], V. Peskov[53], Y. Pestov[5], V. Petráček[40], V. Petrov[111], M. Petrovici[78], C. Petta[29], S. Piano[109], M. Pikna[39], P. Pillot[113], L.O.D.L. Pimentel[81], O. Pinazza[36,104], L. Pinsky[122], D.B. Piyarathna[122], M. Płoskoń[74], M. Planinic[129], J. Pluta[133], S. Pochybova[135], P.L.M. Podesta-Lerma[119], M.G. Poghosyan[85,87], B. Polichtchouk[111], N. Poljak[129], W. Poonsawat[114], A. Pop[78], S. Porteboeuf-Houssais[70], J. Porter[74], J. Pospisil[84], S.K. Prasad[4], R. Preghenella[104,36], F. Prino[110], C.A. Pruneau[134], I. Pshenichnov[56], M. Puccio[27], G. Puddu[25], P. Pujahari[134], V. Punin[99], J. Putschke[134], H. Qvigstad[22], A. Rachevski[109], S. Raha[4], S. Rajput[91], J. Rak[123], A. Rakotozafindrabe[15], L. Ramello[32], F. Rami[55], R. Raniwala[92], S. Raniwala[92], S.S. Räsänen[46], B.T. Rascanu[53], D. Rathee[88], K.F. Read[85,125], K. Redlich[77], R.J. Reed[134], A. Rehman[18], P. Reichelt[53], F. Reidt[94,36], X. Ren[7], R. Renfordt[53], A.R. Reolon[72], A. Reshetin[56], J.-P. Revol[12], K. Reygers[94], V. Riabov[86], R.A. Ricci[73], T. Richert[34], M. Richter[22], P. Riedler[36], W. Riegler[36], F. Riggi[29], C. Ristea[62], E. Rocco[57], M. Rodríguez Cahuantzi[11,2], A. Rodriguez Manso[82], K. Røed[22], E. Rogochaya[66], D. Rohr[43], D. Röhrich[18], R. Romita[124], F. Ronchetti[72,36], L. Ronflette[113], P. Rosnet[70], A. Rossi[36,30], F. Roukoutakis[89], A. Roy[49], C. Roy[55], P. Roy[100], A.J. Rubio Montero[10], R. Rui[26], R. Russo[27], E. Ryabinkin[80], Y. Ryabov[86], A. Rybicki[117],

S. Sadovsky[111] , K. Šafařík[36] , B. Sahlmuller[53] , P. Sahoo[49] , R. Sahoo[49] , S. Sahoo[61] , P.K. Sahu[61] , J. Saini[132] , S. Sakai[72] , M.A. Saleh[134] , J. Salzwedel[20] , S. Sambyal[91] , V. Samsonov[86] , L. Šándor[59] , A. Sandoval[64] , M. Sano[128] , D. Sarkar[132] , P. Sarma[45] , E. Scapparone[104] , F. Scarlassara[30] , C. Schiaua[78] , R. Schicker[94] , C. Schmidt[97] , H.R. Schmidt[35] , S. Schuchmann[53] , J. Schukraft[36] , M. Schulc[40] , T. Schuster[136] , Y. Schutz[36 ,113] , K. Schwarz[97] , K. Schweda[97] , G. Scioli[28] , E. Scomparin[110] , R. Scott[125] , M. Šefčík[41] , J.E. Seger[87] , Y. Sekiguchi[127] , D. Sekihata[47] , I. Selyuzhenkov[97] , K. Senosi[65] , S. Senyukov[3 ,36] , E. Serradilla[10 ,64] , A. Sevcenco[62] , A. Shabanov[56] , A. Shabetai[113] , O. Shadura[3] , R. Shahoyan[36] , M.I. Shahzad[16] , A. Shangaraev[111] , A. Sharma[91] , M. Sharma[91] , M. Sharma[91] , N. Sharma[125] , K. Shigaki[47] , K. Shtejer[9 ,27] , Y. Sibiriak[80] , S. Siddhanta[105] , K.M. Sielewicz[36] , T. Siemiarczuk[77] , D. Silvermyr[34] , C. Silvestre[71] , G. Simatovic[129] , G. Simonetti[36] , R. Singaraju[132] , R. Singh[79] , S. Singha[132 ,79] , V. Singhal[132] , B.C. Sinha[132] , T. Sinha[100] , B. Sitar[39] , M. Sitta[32] , T.B. Skaali[22] , M. Slupecki[123] , N. Smirnov[136] , R.J.M. Snellings[57] , T.W. Snellman[123] , C. Søgaard[34] , J. Song[96] , M. Song[137] , Z. Song[7] , F. Soramel[30] , S. Sorensen[125] , R.D.de Souza[121] , F. Sozzi[97] , M. Spacek[40] , E. Spiriti[72] , I. Sputowska[117] , M. Spyropoulou-Stassinaki[89] , J. Stachel[94] , I. Stan[62] , P. Stankus[85] , G. Stefanek[77] , E. Stenlund[34] , G. Steyn[65] , J.H. Stiller[94] , D. Stocco[113] , P. Strmen[39] , A.A.P. Suaide[120] , T. Sugitate[47] , C. Suire[51] , M. Suleymanov[16] , M. Suljic[26 ,i], R. Sultanov[58] , M. Šumbera[84] , A. Szabo[39] , A. Szanto de Toledo[120 ,i], I. Szarka[39] , A. Szczepankiewicz[36] , M. Szymanski[133] , U. Tabassam[16] , J. Takahashi[121] , G.J. Tambave[18] , N. Tanaka[128] , M.A. Tangaro[33] , M. Tarhini[51] , M. Tariq[19] , M.G. Tarzila[78] , A. Tauro[36] , G. Tejeda Muñoz[2] , A. Telesca[36] , K. Terasaki[127] , C. Terrevoli[30] , B. Teyssier[130] , J. Thäder[74] , D. Thomas[118] , R. Tieulent[130] , A.R. Timmins[122] , A. Toia[53] , S. Trogolo[27] , G. Trombetta[33] , V. Trubnikov[3] , W.H. Trzaska[123] , T. Tsuji[127] , A. Tumkin[99] , R. Turrisi[107] , T.S. Tveter[22] , K. Ullaland[18] , A. Uras[130] , G.L. Usai[25] , A. Utrobicic[129] , M. Vajzer[84] , M. Vala[59] , L. Valencia Palomo[70] , S. Vallero[27] , J. Van Der Maarel[57] , J.W. Van Hoorne[36] , M. van Leeuwen[57] , T. Vanat[84] , P. Vande Vyvre[36] , D. Varga[135] , A. Vargas[2] , M. Vargyas[123] , R. Varma[48] , M. Vasileiou[89] , A. Vasiliev[80] , A. Vauthier[71] , V. Vechernin[131] , A.M. Veen[57] , M. Veldhoen[57] , A. Velure[18] , M. Venaruzzo[73] , E. Vercellin[27] , S. Vergara Limón[2] , R. Vernet[8] , M. Verweij[134] , L. Vickovic[116] , G. Viesti[30 ,i], J. Viinikainen[123] , Z. Vilakazi[126] , O. Villalobos Baillie[101] , A. Villatoro Tello[2] , A. Vinogradov[80] , L. Vinogradov[131] , Y. Vinogradov[99 ,i], T. Virgili[31] , V. Vislavicius[34] , Y.P. Viyogi[132] , A. Vodopyanov[66] , M.A. Völkl[94] , K. Voloshin[58] , S.A. Voloshin[134] , G. Volpe[33] , B. von Haller[36] , I. Vorobyev[37 ,93] , D. Vranic[97 ,36] , J. Vrláková[41] , B. Vulpescu[70] , B. Wagner[18] , J. Wagner[97] , H. Wang[57] , M. Wang[7 ,113] , D. Watanabe[128] , Y. Watanabe[127] , M. Weber[36 ,112] , S.G. Weber[97] , D.F. Weiser[94] , J.P. Wessels[54] , U. Westerhoff[54] , A.M. Whitehead[90] , J. Wiechula[35] , J. Wikne[22] , G. Wilk[77] , J. Wilkinson[94] , M.C.S. Williams[104] , B. Windelband[94] , M. Winn[94] , H. Yang[57] , P. Yang[7] , S. Yano[47] , Z. Yasin[16] , Z. Yin[7] , H. Yokoyama[128] , I.-K. Yoo[96] , J.H. Yoon[50] , V. Yurchenko[3] , I. Yushmanov[80] , A. Zaborowska[133] , V. Zaccolo[81] , A. Zaman[16] , C. Zampolli[36 ,104] , H.J.C. Zanoli[120] , S. Zaporozhets[66] , N. Zardoshti[101] , A. Zarochentsev[131] , P. Závada[60] , N. Zaviyalov[99] , H. Zbroszczyk[133] , I.S. Zgura[62] , M. Zhalov[86] , H. Zhang[18] , X. Zhang[74] , Y. Zhang[7] , C. Zhang[57] , Z. Zhang[7] , C. Zhao[22] , N. Zhigareva[58] , D. Zhou[7] , Y. Zhou[81] , Z. Zhou[18] , H. Zhu[18] , J. Zhu[113 ,7] , A. Zichichi[28 ,12] , A. Zimmermann[94] , M.B. Zimmermann[54 ,36] , G. Zinovjev[3] , M. Zyzak[43]

Affiliation notes

[i] Deceased
[ii] Also at: Georgia State University, Atlanta, Georgia, United States
[iii] Also at: Also at Department of Applied Physics, Aligarh Muslim University, Aligarh, India
[iv] Also at: M.V. Lomonosov Moscow State University, D.V. Skobeltsyn Institute of Nuclear, Physics, Moscow, Russia

Collaboration Institutes

[1] A.I. Alikhanyan National Science Laboratory (Yerevan Physics Institute) Foundation, Yerevan, Armenia
[2] Benemérita Universidad Autónoma de Puebla, Puebla, Mexico
[3] Bogolyubov Institute for Theoretical Physics, Kiev, Ukraine
[4] Bose Institute, Department of Physics and Centre for Astroparticle Physics and Space Science (CAPSS), Kolkata, India
[5] Budker Institute for Nuclear Physics, Novosibirsk, Russia
[6] California Polytechnic State University, San Luis Obispo, California, United States
[7] Central China Normal University, Wuhan, China
[8] Centre de Calcul de l'IN2P3, Villeurbanne, France
[9] Centro de Aplicaciones Tecnológicas y Desarrollo Nuclear (CEADEN), Havana, Cuba

[10] Centro de Investigaciones Energéticas Medioambientales y Tecnológicas (CIEMAT), Madrid, Spain
[11] Centro de Investigación y de Estudios Avanzados (CINVESTAV), Mexico City and Mérida, Mexico
[12] Centro Fermi - Museo Storico della Fisica e Centro Studi e Ricerche "Enrico Fermi", Rome, Italy
[13] Chicago State University, Chicago, Illinois, USA
[14] China Institute of Atomic Energy, Beijing, China
[15] Commissariat à l'Energie Atomique, IRFU, Saclay, France
[16] COMSATS Institute of Information Technology (CIIT), Islamabad, Pakistan
[17] Departamento de Física de Partículas and IGFAE, Universidad de Santiago de Compostela, Santiago de Compostela, Spain
[18] Department of Physics and Technology, University of Bergen, Bergen, Norway
[19] Department of Physics, Aligarh Muslim University, Aligarh, India
[20] Department of Physics, Ohio State University, Columbus, Ohio, United States
[21] Department of Physics, Sejong University, Seoul, South Korea
[22] Department of Physics, University of Oslo, Oslo, Norway
[23] Dipartimento di Elettrotecnica ed Elettronica del Politecnico, Bari, Italy
[24] Dipartimento di Fisica dell'Università 'La Sapienza' and Sezione INFN Rome, Italy
[25] Dipartimento di Fisica dell'Università and Sezione INFN, Cagliari, Italy
[26] Dipartimento di Fisica dell'Università and Sezione INFN, Trieste, Italy
[27] Dipartimento di Fisica dell'Università and Sezione INFN, Turin, Italy
[28] Dipartimento di Fisica e Astronomia dell'Università and Sezione INFN, Bologna, Italy
[29] Dipartimento di Fisica e Astronomia dell'Università and Sezione INFN, Catania, Italy
[30] Dipartimento di Fisica e Astronomia dell'Università and Sezione INFN, Padova, Italy
[31] Dipartimento di Fisica 'E.R. Caianiello' dell'Università and Gruppo Collegato INFN, Salerno, Italy
[32] Dipartimento di Scienze e Innovazione Tecnologica dell'Università del Piemonte Orientale and Gruppo Collegato INFN, Alessandria, Italy
[33] Dipartimento Interateneo di Fisica 'M. Merlin' and Sezione INFN, Bari, Italy
[34] Division of Experimental High Energy Physics, University of Lund, Lund, Sweden
[35] Eberhard Karls Universität Tübingen, Tübingen, Germany
[36] European Organization for Nuclear Research (CERN), Geneva, Switzerland
[37] Excellence Cluster Universe, Technische Universität München, Munich, Germany
[38] Faculty of Engineering, Bergen University College, Bergen, Norway
[39] Faculty of Mathematics, Physics and Informatics, Comenius University, Bratislava, Slovakia
[40] Faculty of Nuclear Sciences and Physical Engineering, Czech Technical University in Prague, Prague, Czech Republic
[41] Faculty of Science, P.J. Šafárik University, Košice, Slovakia
[42] Faculty of Technology, Buskerud and Vestfold University College, Vestfold, Norway
[43] Frankfurt Institute for Advanced Studies, Johann Wolfgang Goethe-Universität Frankfurt, Frankfurt, Germany
[44] Gangneung-Wonju National University, Gangneung, South Korea
[45] Gauhati University, Department of Physics, Guwahati, India
[46] Helsinki Institute of Physics (HIP), Helsinki, Finland
[47] Hiroshima University, Hiroshima, Japan
[48] Indian Institute of Technology Bombay (IIT), Mumbai, India
[49] Indian Institute of Technology Indore, Indore (IITI), India
[50] Inha University, Incheon, South Korea
[51] Institut de Physique Nucléaire d'Orsay (IPNO), Université Paris-Sud, CNRS-IN2P3, Orsay, France
[52] Institut für Informatik, Johann Wolfgang Goethe-Universität Frankfurt, Frankfurt, Germany
[53] Institut für Kernphysik, Johann Wolfgang Goethe-Universität Frankfurt, Frankfurt, Germany
[54] Institut für Kernphysik, Westfälische Wilhelms-Universität Münster, Münster, Germany
[55] Institut Pluridisciplinaire Hubert Curien (IPHC), Université de Strasbourg, CNRS-IN2P3, Strasbourg, France
[56] Institute for Nuclear Research, Academy of Sciences, Moscow, Russia
[57] Institute for Subatomic Physics of Utrecht University, Utrecht, Netherlands
[58] Institute for Theoretical and Experimental Physics, Moscow, Russia
[59] Institute of Experimental Physics, Slovak Academy of Sciences, Košice, Slovakia
[60] Institute of Physics, Academy of Sciences of the Czech Republic, Prague, Czech Republic

[61] Institute of Physics, Bhubaneswar, India
[62] Institute of Space Science (ISS), Bucharest, Romania
[63] Instituto de Ciencias Nucleares, Universidad Nacional Autónoma de México, Mexico City, Mexico
[64] Instituto de Física, Universidad Nacional Autónoma de México, Mexico City, Mexico
[65] iThemba LABS, National Research Foundation, Somerset West, South Africa
[66] Joint Institute for Nuclear Research (JINR), Dubna, Russia
[67] Konkuk University, Seoul, South Korea
[68] Korea Institute of Science and Technology Information, Daejeon, South Korea
[69] KTO Karatay University, Konya, Turkey
[70] Laboratoire de Physique Corpusculaire (LPC), Clermont Université, Université Blaise Pascal, CNRS–IN2P3, Clermont-Ferrand, France
[71] Laboratoire de Physique Subatomique et de Cosmologie, Université Grenoble-Alpes, CNRS-IN2P3, Grenoble, France
[72] Laboratori Nazionali di Frascati, INFN, Frascati, Italy
[73] Laboratori Nazionali di Legnaro, INFN, Legnaro, Italy
[74] Lawrence Berkeley National Laboratory, Berkeley, California, United States
[75] Moscow Engineering Physics Institute, Moscow, Russia
[76] Nagasaki Institute of Applied Science, Nagasaki, Japan
[77] National Centre for Nuclear Studies, Warsaw, Poland
[78] National Institute for Physics and Nuclear Engineering, Bucharest, Romania
[79] National Institute of Science Education and Research, Bhubaneswar, India
[80] National Research Centre Kurchatov Institute, Moscow, Russia
[81] Niels Bohr Institute, University of Copenhagen, Copenhagen, Denmark
[82] Nikhef, Nationaal instituut voor subatomaire fysica, Amsterdam, Netherlands
[83] Nuclear Physics Group, STFC Daresbury Laboratory, Daresbury, United Kingdom
[84] Nuclear Physics Institute, Academy of Sciences of the Czech Republic, Řež u Prahy, Czech Republic
[85] Oak Ridge National Laboratory, Oak Ridge, Tennessee, United States
[86] Petersburg Nuclear Physics Institute, Gatchina, Russia
[87] Physics Department, Creighton University, Omaha, Nebraska, United States
[88] Physics Department, Panjab University, Chandigarh, India
[89] Physics Department, University of Athens, Athens, Greece
[90] Physics Department, University of Cape Town, Cape Town, South Africa
[91] Physics Department, University of Jammu, Jammu, India
[92] Physics Department, University of Rajasthan, Jaipur, India
[93] Physik Department, Technische Universität München, Munich, Germany
[94] Physikalisches Institut, Ruprecht-Karls-Universität Heidelberg, Heidelberg, Germany
[95] Purdue University, West Lafayette, Indiana, United States
[96] Pusan National University, Pusan, South Korea
[97] Research Division and ExtreMe Matter Institute EMMI, GSI Helmholtzzentrum für Schwerionenforschung, Darmstadt, Germany
[98] Rudjer Bošković Institute, Zagreb, Croatia
[99] Russian Federal Nuclear Center (VNIIEF), Sarov, Russia
[100] Saha Institute of Nuclear Physics, Kolkata, India
[101] School of Physics and Astronomy, University of Birmingham, Birmingham, United Kingdom
[102] Sección Física, Departamento de Ciencias, Pontificia Universidad Católica del Perú, Lima, Peru
[103] Sezione INFN, Bari, Italy
[104] Sezione INFN, Bologna, Italy
[105] Sezione INFN, Cagliari, Italy
[106] Sezione INFN, Catania, Italy
[107] Sezione INFN, Padova, Italy
[108] Sezione INFN, Rome, Italy
[109] Sezione INFN, Trieste, Italy
[110] Sezione INFN, Turin, Italy
[111] SSC IHEP of NRC Kurchatov institute, Protvino, Russia
[112] Stefan Meyer Institut für Subatomare Physik (SMI), Vienna, Austria
[113] SUBATECH, Ecole des Mines de Nantes, Université de Nantes, CNRS-IN2P3, Nantes, France

[114] Suranaree University of Technology, Nakhon Ratchasima, Thailand
[115] Technical University of Košice, Košice, Slovakia
[116] Technical University of Split FESB, Split, Croatia
[117] The Henryk Niewodniczanski Institute of Nuclear Physics, Polish Academy of Sciences, Cracow, Poland
[118] The University of Texas at Austin, Physics Department, Austin, Texas, USA
[119] Universidad Autónoma de Sinaloa, Culiacán, Mexico
[120] Universidade de São Paulo (USP), São Paulo, Brazil
[121] Universidade Estadual de Campinas (UNICAMP), Campinas, Brazil
[122] University of Houston, Houston, Texas, United States
[123] University of Jyväskylä, Jyväskylä, Finland
[124] University of Liverpool, Liverpool, United Kingdom
[125] University of Tennessee, Knoxville, Tennessee, United States
[126] University of the Witwatersrand, Johannesburg, South Africa
[127] University of Tokyo, Tokyo, Japan
[128] University of Tsukuba, Tsukuba, Japan
[129] University of Zagreb, Zagreb, Croatia
[130] Université de Lyon, Université Lyon 1, CNRS/IN2P3, IPN-Lyon, Villeurbanne, France
[131] V. Fock Institute for Physics, St. Petersburg State University, St. Petersburg, Russia
[132] Variable Energy Cyclotron Centre, Kolkata, India
[133] Warsaw University of Technology, Warsaw, Poland
[134] Wayne State University, Detroit, Michigan, United States
[135] Wigner Research Centre for Physics, Hungarian Academy of Sciences, Budapest, Hungary
[136] Yale University, New Haven, Connecticut, United States
[137] Yonsei University, Seoul, South Korea
[138] Zentrum für Technologietransfer und Telekommunikation (ZTT), Fachhochschule Worms, Worms, Germany